photon emission computed tomography (SPECT). Biol. Pharm. Bull. 32, 337–340.

Olincy, A., Stevens, K.E., 2007. Treating schizophrenia symptoms with an α7 nicotinic agonist, from mice to men. Biochem. Pharmacol. 74, 1192–1201.

Pichat, P., Bergis, O.E., Terranova, J.P., Urani, A., Duarte, C., Santucci, V., Gueudet, C., Voltz, C., Steinberg, R., Stemmelin, J., Oury-Donat, F., Avenet, P., Griebel, G., Scatton, B., 2007. SSR180711, a novel selective α7 nicotinic receptor partial agonist: (II) efficacy in experimental models predictive of activity against cognitive symptoms of schizophrenia Neuropsychopharmacology 32, 17–34.

Quik, M., Polonskaya, Y., Gillespie, A., Jakowec, M., Lloyd, G.K., Langston, J.W., 2000. Localization of nicotinic receptor subunit mRNAs in monkey brain by *in situ* hybridization. J. Comp. Neurol. 425, 58–69.

Séguéla, P., Wadiche, J., Dineley-Miller, K., Dani, J.A., Patrick, J.W., 1993. Molecular cloning, functional properties, and distribution of rat brain α7: a nicotinic cation channel highly permeable to calcium. J. Neurosci. 13, 596–604.

Simosky, J.K., Stevens, K.E., Freedman, R., 2002. Nicotinic agonists and psychosis. Curr. Drug Targets CNS Neurol. Disord. 1, 149–162.

Thomsen, M.S., Christensen, D.Z., Hansen, H.H., Redrobe, J.P., Mikkelsen, J.D., 2009. α7 Nicotinic acetylcholine receptor activation prevents behavioral and molecular changes induced by repeated phencyclidine treatment. Neuropharmacology 56, 1001–1009.

Tietje, K.R., Anderson, D.J., Bitner, R.S., Blomme, E.A., Brackemeyer, P.J., Briggs, C.A., Browman, K.E., Bury, D., Curzon, P., Drescher, K.U., Frost, J.M., Fryer, R.M., Fox, G.B., Gronlien, J.H., Håkerud, M., Gubbins, E.J., Halm, S., Harris, R., Helfrich, R.J., Kohlhaas, K.L., Law, D., Malysz, J., Marsh, K.C., Martin, R.L., Meyer, M.D., Molesky, A.L., Nikkel, A.L., Otte, S., Pan, L., Puttfarcken, P.S., Radek, R.J., Robb, H.M., Spies, E., Thorin-Hagene, K., Waring, J.F., Ween, H., Xu, H., Gopalakrishnan, M., Bunnelle, W.H., 2008. Preclinical characterization of A-582941: a novel α7 neuronal nicotinic receptor agonist with broad spectrum cognition-enhancing properties. CNS Neurosci. Ther. 14, 65–82.

Toyohara, J., Hashimoto, K., 2010. α7 Nicotinic receptor agonists: potential therapeutic drugs for treatment of cognitive impairments in schizophrenia and Alzheimer's disease. Open Med. Chem. J. 4, 37–56.

Toyohara, J., Sakata, M., Wu, J., Ishikawa, M., Oda, K., Ishii, K., Iyo, M., Hashimoto, K., Ishiwata, K., 2009. Preclinical and the first clinical studies on [^{11}C]CHIBA-1001 for mapping α7 nicotinic receptors by positron emission tomography. Ann. Nucl. Med. 23, 301–309.

Toyohara, J., Ishiwata, K., Sakata, M., Wu, J., Nishiyama, S., Tsukada, H., Hashimoto, K., 2010. *In vivo* evaluation of α7 nicotinic acetylcholine receptor agonists [^{11}C]A-582941 and [^{11}C]A-844606 in mice and conscious monkeys. PLoS ONE 5, e8961.

Toyohara, J., Wu, J., Hashimoto, K., 2010. Recent development of radioligands for imaging α7 nicotinic acetylcholine receptors in the brain. Curr. Top. Med. Chem.

Van Kampen, M., Selbach, K., Schneider, R., Schiegel, E., Boess, F., Schreiber, R., 2004. AR-R 17779 improves social recognition in rats by activation of nicotinic α7 receptors. Psychopharmacology (Berl) 172, 375–383.

Wang, H.Y., Stucky, A., Liu, J., Shen, C., Trocme-Thibierge, C., Morain, P., 2009. Dissociating beta-amyloid from α7 nicotinic acetylcholine receptor by a novel therapeutic agent, S 24795, normalizes α7 nicotinic acetylcholine and NMDA receptor function in Alzheimer's disease brain. J. Neurosci. 29, 10961–10973.

Wevers, A., Burghaus, L., Moser, N., Witter, B., Steinlein, O.K., Schütz, U., Achnitz, B., Krempel, U., Nowacki, S., Pilz, K., Stoodt, J., Lindstrom, J., De Vos, R.A., Jansen Steur, E.N., Schröder, H., 2000. Expression of nicotinic acetylcholine receptors in Alzheimer's disease: postmortem investigations and experimental approaches. Behav. Brain Res. 113, 207–215.

Wishka, D.G., Walker, D.P., Yates, K.M., Reitz, S.C., Jia, S., Myers, J.K., Olson, K.L., Jacobsen, E.J., Wolfe, M.L., Groppi, V.E., Hanchar, A.J., Thomburgh, B.A., Cortes-Burgos, L.A., Wong, E.H., Staton, B.A., Raub, T.J., Higdon, N.R., Wall, T.M., Hurst, R.S., Walters, R.R., Hoffmann, W.E., Hajos, M., Franklin, S., Carey, G., Gold, L.H., Cook, K.K., Sands, S.B., Zhao, S.X., Soglia, J.R., Kalgutkar, A.S., Americ, S.P., Rogers, B.N., 2006. Discovery of N-[(3R)-1-azabicyclo [2.2.2]oct-3-yl]furo[2, 3-c]pyridine-5-carboxamide, an agonist of the α7 nicotinic acetylcholine receptor, for the potential treatment of cognitive deficits in schizophrenia: synthesis and structure–activity relationship. J. Med. Chem. 49, 4425–4436.

Young, J.W., Finlayson, K., Spratt, C., Marston, H.M., Crawford, N., Kelly, J.S., Sharkey, J., 2004. Nicotine improves sustained attention in mice: evidence for involvement of the α7 nicotinic acetylcholine receptor. Neuropsychopharmacology 29, 891–900.

Young, J.W., Crawford, N., Kelly, J.S., Kerr, L.E., Marston, H.M., Spratt, C., Finlayson, K., Sharkey, J., 2007. Impaired attention is central to the cognitive deficits observed in α7 deficient mice. Eur. Neuropsychopharmacol. 17, 145–155.

CASE REPORT

Improvement of Asymmetrical Temporal Blood Flow in Refractory Oral Somatic Delusion After Successful Electroconvulsive Therapy

Akihito Uezato, MD, PhD,†‡ Naoki Yamamoto, MD, PhD,* Akeo Kurumaji, MD, PhD,* Akira Toriihara, MD, PhD,§ Yojiro Umezaki, DDS,|| Akira Toyofuku, DDS, PhD,|| and Toru Nishikawa, MD, PhD**

Abstract: Oral cenesthopathy is a somatic delusion in the oral area and categorized as delusional disorder, somatic type. Patients experience unusual and annoying sensations in the mouth such as pulling on the teeth, moving teeth, overly secreting mucus, tingling and pain, and so on, without a somatic base. The condition is usually treatment-resistant and impairs patients' quality of life. We report a case of oral cenesthopathy successfully treated with the modified electroconvulsive therapy, who demonstrated altered regional cerebral blood flow before and after the treatment detected by single-photon emission computed tomography.

Key Words: somatic-type delusional disorder, oral cenesthopathy, modified electroconvulsive therapy, SPECT, temporal lobe

(*J ECT* 2012;28: 50–51)

Oral cenesthopathy is a somatic delusion in the oral area and categorized as delusional disorder, somatic type. Patients experience unusual and annoying sensations in the mouth such as pulling on the teeth, moving teeth, overly secreting mucus, tingling and pain, and so on, without a somatic base. This condition draws clinical attentions because patients usually undergo dental service claiming the treatment itself worsens their symptoms. Not only their eating or speaking is impaired, but also their quality of life is extremely disturbed because of the symptoms. Antidepressants or antipsychotics have been reported to alleviate the condition, but it is usually treatment-resistant. We report a case of oral somatic delusion successfully treated with the modified electroconvulsive therapy (mECT), who demonstrated altered regional cerebral blood flow before and after the treatment detected by single-photon emission computed tomography (SPECT).

CASE REPORT

Mrs A. was a 53-year-old Japanese woman with a history of mild depression. In 2005, she started to have unusual sensations in her mouth feeling "something like water or bubble coming out of the teeth and gums," accompanied by mild depressive symptoms. Although her depression improved within a few months, the annoying sensations in the mouth continued. A mouthpiece prescribed by a dentist was somewhat effective because she felt it "dammed up" the water and bubble. In 2007, she visited the university hospital of dentistry. The trials of antidepressants and antipsychotics resulted in a minimal improvement. In the evaluation at our psychiatry department in 2010, Mrs A. claimed "I can no more lie down on the bed because the gravity helps water and bubbles come out more" and stopped eating. No objective abnormalities were observed in the oral area. Brain magnetic resonance imaging showed no abnormalities. Single-photon emission computed tomography images demonstrated distinct asymmetry with the hyperperfusion in the right temporal lobe compared with the left (Fig. 1, left). Following unsuccessful treatment with antidepressants and antipsychotics, we introduced mECT. The electrical stimulator used was Thymatron System IV (Somatics, LLC, Lake Bluff, Ill). Bilateral ECT with brief pulse was performed twice a week for a total of 10 times. The seizure threshold was determined by the half-age method during the first ECT session. Propofol (0.8 mg/kg at the first ECT session) by intravenous bolus was used for anesthesia, followed by intravenously administered succinylcholine (1 mg/kg) as a muscle relaxant. The quantity of the anesthetic agent was revised in the subsequent sessions in consideration of the anesthetic effect. The average stimulus dose delivered was 70.5%, which is equivalent to 355 mC. The average seizure durations were 14.4 and 29.7 seconds, measured by observing the motor convulsion and the electroencephalogram, respectively. The medications at the pretreatment SPECT evaluation include perospirone 20 mg, lorazepam 3 mg, flunitrazepam 1 mg, brotizolam 0.25 mg, and biperiden 3 mg. All medications were maintained on the same dosage until the posttreatment SPECT evaluation except perospirone, which was increased to 32 mg before starting mECT. When Mrs A. felt the symptoms in her oral area were alleviated after the treatment with mECT, the perfusion asymmetry disappeared in SPECT images (Fig. 1, right).

DISCUSSION

Regarding perfusion asymmetry, the finding of the right temporal hyperperfusion in the present case was similar to those of previously reported cases of oral somatic delusion, which demonstrated hypoperfusion in the left temporal and parietal lobes.[1,2] Similar to our case, their asymmetry was normalized after the successful treatment by paroxetine or mECT. A recent epilepsy case series reported that the majority of patients with postictal psychoses demonstrated increased right temporal or decreased left temporal perfusion detected by SPECT.[3] Regardless of whether right- or left-sided pathology, right-sided temporal predominance was characteristic. As the functional asymmetry

From the *Section of Psychiatry and Behavioral Sciences and †Department of Sleep Modulatory Medicine, Tokyo Medical and Dental University Graduate School, Tokyo, Japan; ‡Department of Psychiatry and Behavioral Neurobiology, University of Alabama at Birmingham, Birmingham, AL; and §Department of Diagnostic Radiology and Oncology and ||Section of Psychosomatic Dentistry, Tokyo Medical and Dental University Graduate School, Tokyo, Japan.

Received for publication July 1, 2011; accepted July 18, 2011.

Reprints: Toru Nishikawa, MD, PhD, Section of Psychiatry and Behavioral Sciences, Tokyo Medical and Dental University Graduate School, 1-5-45, Yushima, Bunkyo-ku, Tokyo 113-8519, Japan (e-mail: tnis.psyc@tmd.ac.jp).

There is no financial relationship or other affiliations relevant to the subject of this work. None of the named authors have any financial relationship with commercial interests.

DOI: 10.1097/YCT.0b013e31822e581e

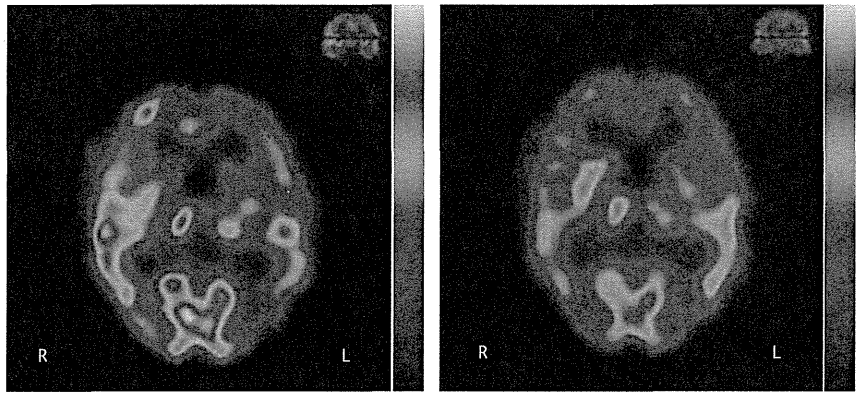

FIGURE 1. Single-photon emission computed tomography (technetium Tc 99m ethyl cysteinate dimer) images before (left) and after (right) the treatment.

has also been suggested in schizophrenia,[4] the asymmetricity shared among these conditions might represent their pathophysiology, such as abnormal sensory processing. Oral cenesthopathy has been likely underestimated because its concept is not well established, but mental health providers often encounter it especially through consultations by general physicians or dentists and struggle with treatment. Acknowledging its symptoms and imaging patterns should further improve care of patients.

REFERENCES

1. Ota M, Mizukami K, Katano T, et al. A case of delusional disorder, somatic type with remarkable improvement of clinical symptoms and single photon emission computed tomography findings following modified electroconvulsive therapy. *Prog Neuropsychopharmacol Biol Psychiatry.* 2003;27:881–884.
2. Hayashi H, Oshino S, Ishikawa J, et al. Paroxetine treatment of delusional disorder, somatic type. *Hum Psychopharmacol.* 2004;19:351–352.
3. Oshima T, Motooka H, Kanemoto K. SPECT findings during postictal psychoses: predominance of relative increase of perfusion in right temporal lobe. *Epilepsia.* 2011;52:1192–1194.
4. Ke M, Zou R, Shen H, et al. Bilateral functional asymmetry disparity in positive and negative schizophrenia revealed by resting-state fMRI. *Psychiatry Res.* 2010;182:30–39.

No.32
Journal of Nuclear Medicine, published on June 11, 2012 as doi:10.2967/jnumed.111.101626

Quantification of Dopamine Transporter in Human Brain Using PET with ^{18}F-FE-PE2I

Takeshi Sasaki[1,2], Hiroshi Ito[1,3], Yasuyuki Kimura[1], Ryosuke Arakawa[1], Harumasa Takano[1], Chie Seki[3], Fumitoshi Kodaka[1], Saori Fujie[1], Keisuke Takahata[1], Tsuyoshi Nogami[1], Masayuki Suzuki[1], Hironobu Fujiwara[1], Hidehiko Takahashi[1], Ryuji Nakao[4], Toshimitsu Fukumura[5], Andrea Varrone[4], Christer Halldin[4], Toru Nishikawa[2], and Tetsuya Suhara[1]

[1]Molecular Neuroimaging Program, Molecular Imaging Center, National Institute of Radiological Sciences, Chiba, Japan; [2]Department of Psychiatry and Behavioral Sciences, Tokyo Medical and Dental University Graduate School, Tokyo, Japan; [3]Biophysics Program, Molecular Imaging Center, National Institute of Radiological Sciences, Chiba, Japan; [4]Karolinska Institutet, Department of Clinical Neuroscience, Centre for Psychiatry Research, Karolinska Hospital, Stockholm, Sweden; and [5]Molecular Probe Program, Molecular Imaging Center, National Institute of Radiological Sciences, Chiba, Japan

^{18}F-(*E*)-*N*-(3-iodoprop-2*E*-enyl)-2β-carbofluoroethoxy-3β-(4-methylphenyl)nortropane (^{18}F-FE-PE2I) is a new PET radioligand with a high affinity and selectivity for the dopamine transporter (DAT). In nonhuman primates, ^{18}F-FE-PE2I showed faster kinetics and less production of radiometabolites that could potentially permeate the blood–brain barrier than did ^{11}C-PE2I. The aims of this study were to examine the quantification of DAT using ^{18}F-FE-PE2I and to assess the effect of radiometabolites of ^{18}F-FE-PE2I on the quantification in healthy humans. **Methods:** A 90-min dynamic PET scan was obtained for 10 healthy men after intravenous injection of ^{18}F-FE-PE2I. Kinetic compartment model analysis with a metabolite-corrected arterial input function was performed. The effect of radiometabolites on the quantification was evaluated by time-stability analyses. The simplified reference tissue model (SRTM) method with the cerebellum as a reference region was evaluated as a noninvasive method of quantification. **Results:** After the injection of ^{18}F-FE-PE2I, the whole-brain radioactivity showed a high peak (~3–5 standardized uptake value) and fast washout. The radioactive uptake of ^{18}F-FE-PE2I in the brain was according to the relative density of the DAT (striatum > midbrain > thalamus). The cerebellum showed the lowest uptake. Tissue time–activity curves were well described by the 2-tissue-compartment model (TCM), as compared with the 1-TCM, for all subjects in all regions. Time stability analysis showed stable estimation of total distribution volume with 60-min or longer scan durations, indicating the small effect of radiometabolites. Binding potentials in the striatum and midbrain were well estimated by the SRTM method, with modest intersubject variability. Although the SRTM method yielded a slight underestimation and overestimation in regions with high and low DAT densities, respectively, binding potentials by the SRTM method were well correlated to the estimates by the indirect kinetic method with 2-TCM. **Conclusion:** ^{18}F-FE-PE2I is a promising PET radioligand for quantifying DAT. The binding potentials could be reliably estimated in both the striatum and midbrain using both the indirect kinetic and SRTM methods with a scan duration of 60 min. Although radiometabolites of ^{18}F-FE-PE2I in plasma possibly introduced some effects on the radioactivity in the brain, the effects on estimated binding potential were likely to be small.

Key Words: ^{18}F-FE-PE2I; positron emission tomography; dopamine transporter; kinetic modeling; radiometabolite

J Nucl Med 2012; 53:1–9
DOI: 10.2967/jnumed.111.101626

Dopamine transporter (DAT) plays a crucial role in the regulation of dopamine concentration in the synaptic cleft by dopamine reuptake. Changes in the density and function of DAT have been reported in various neuropsychiatric disorders, such as Parkinson disease (*1*), Huntington disease (*2*), attention-deficit/hyperactivity disorder (*3*), autism (*4*), and schizophrenia (*5*). Although DAT ligands for SPECT have been widely used in clinical practice, developing a useful radioligand for PET—which has higher resolution and better ability of quantification than SPECT—is the key to assessing its role in the pathophysiology of these diseases and to developing new therapeutic approaches for them.

Several radioligands for imaging DAT have been developed and used for PET. Among ^{11}C-labeled radioligands, ^{11}C-cocaine (*6*), ^{11}C-WIN35,428 (CFT) (*7*), ^{11}C-β-CIT (*8*), and ^{11}C-DL-threo-methylphenidate (*9*) have relatively low affinity for DAT or have slow kinetics in the high-DAT-density regions. ^{11}C-altropane has high affinity and selectivity for DAT (*10*), but the kinetics in the human brain have not been reported in detail to our knowledge. The ^{18}F-labeled radioligands that have been studied in humans so far include ^{18}F-CFT (^{18}F-WIN35,428) (*11*), *N*-3-fluoropropyl-2-β-carboxymethoxy-3-β-(4-iodophenyl)

Received Dec. 6, 2011; revision accepted Feb. 27, 2012.
For correspondence or reprints contact: Hitoshi Ito, Biophysics Program, Molecular Imaging Center, National Institute of Radiological Sciences, 4-9-1, Anagawa, Inage-ku, Chiba, 263-8555, Japan.
E-mail: hito@nirs.go.jp
Published online ■■■■.

nortropane (^{18}F-FPCIT) (*12*), and 2β-carbomethoxy-3β-(4-chlorophenyl)-8-(2-fluoroethyl)nortropane (^{18}F-FECNT) (*13*). All of them have high affinity and selectivity for DAT, but the kinetics are relatively slow, and more than 90 min are needed to reach peak uptake in the striatum.

Recently, a new ligand, *N*-(3-iodoprop-2*E*-enyl)-2β-carbomethoxy-3β-(4-methylphenyl)nortropane (PE2I), with a high affinity for DAT (inhibition constant, 17 nM) and good selectivity, was developed (*14,15*). In human PET studies, ^{11}C-PE2I showed a high specific-to-nonspecific ratio (*15–18*). However, 2 problems have been reported in quantifying DAT with ^{11}C-PE2I. First, because of the relatively slow kinetics of ^{11}C-PE2I in the striatum, reference tissue methods severely (~50%) underestimated DAT binding in this region, compared with those by the methods with arterial input function (*16,17*). Second, a radiometabolite of ^{11}C-PE2I has been found to cross the blood–brain barrier (BBB) in rats, thus potentially reducing the accuracy of the quantification of DAT (*19*).

A fluoroethyl analog of PE2I, ^{18}F-(*E*)-*N*-(3-iodoprop-2*E*-enyl)-2β-carbofluoroethoxy-3β-(4-methylphenyl)nortropane (^{18}F-FE-PE2I) (inhibition constant, 12 nM), has recently been developed and evaluated in nonhuman primates (*20*). In monkeys, ^{18}F-FE-PE2I was more favorable for the quantitative analysis of DAT, because it showed faster kinetics and less production of BBB-permeable radiometabolites than did ^{11}C-PE2I. The quantification of DAT with ^{18}F-FE-PE2I was less biased than that with ^{11}C-PE2I (*21*).

The aims of this study were to examine the method for quantification of DAT using ^{18}F-FE-PE2I and to assess the effect of radiometabolites of ^{18}F-FE-PE2I on the quantification in healthy humans.

MATERIALS AND METHODS

Subjects

Ten healthy men (mean age ± SD, 28.1 ± 6.9 y; age range, 20–39 y) participated in this study. All subjects were free of any somatic, neurologic, or psychiatric disorders. The study was approved by the Ethics and Radiation Safety Committee of the National Institute of Radiologic Sciences, Chiba, Japan. Written informed consent was obtained from all subjects before their inclusion in the study.

PET Procedure

^{18}F-FE-PE2I was synthesized from its acid precursor through a reaction with ^{18}F-2-bromo-1-fluoroethane in dimethylformamide and sodium hydroxide in *N,N*-dimethylformamide, as previously described (*22*).

A 90-min dynamic scan was obtained for each subject after a 1-min intravenous injection of ^{18}F-FE-PE2I using a PET scanner system (ECAT EXACT HR+; CTI-Siemens) The scan protocol consisted of 9 frames of 20 s, 5 frames of 1 min, 4 frames of 2 min, 12 frames of 4 min, and 5 frames of 6 min. The injected dose and specific activity were 183.0 ± 9.3 MBq and 146.1 ± 98.7 GBq/μmol at the time of injection, respectively. A head holder was used to minimize head movements. Scatter correction was performed. Attenuation correction was based on a transmission scan using a $^{68/68}$Ge/Ga source.

Arterial Blood Sampling and Metabolite Analysis

Arterial blood samples were taken manually 32 times after the injection of radioligand to obtain an arterial input function. Each blood sample was centrifuged to obtain plasma and blood cell fractions, and the concentration of radioactivity in whole blood and plasma was measured.

The fractions of the parent and its radiometabolites in plasma were determined by high-performance liquid chromatography (HPLC) from 10 blood samples for each subject. Each plasma sample had acetonitrile added and then was centrifuged. The supernatant of the centrifuged sample was subjected to radio-HPLC analysis (column, μBondapak C18 [Waters]). Acetonitrile (90%) (A) and phosphoric acid (0.01 M) (B) were used as mobile phases, with a flow rate of 6.0 mL/min. Gradient elution was used with the following gradient profile: 0–4.5 min, 25/75–70/30 A/B; 4.5–8.0 min, 70/30–25/75 A/B; and 8.0–10.0 min, 25/75–25/75 A/B. Linear interpolation was used to calculate the fractions of the parent and radiometabolites for the blood samples without metabolite analysis.

Image Analysis

T1-weighted MR images acquired with a 1.5-T MRI scanner (Gyroscan NT; Philips) (1-mm-slice axial images; repetition time, 21 ms; echo time, 9.2 ms; and flip angle, 30°) were coregistered to the corresponding PET images. Manually drawn volumes of interest were based on the anatomic information of MR images. Then, these volumes of interest were applied to the dynamic PET images to extract time–activity curves for the putamen, caudate, ventral midbrain (including the substantia nigra and ventral tegmental area), thalamus, and cerebellum. All image and kinetic analyses were performed using PMOD (version 3.0; PMOD Technologies).

Kinetic Analysis

Standard 1- and 2-tissue-compartment models (TCMs) (*18,23*) with an arterial input function (concentration of the parent in plasma) were used to estimate rate constants and total distribution volume (V_T) by an iterative nonlinear least-squares curve-fitting procedure without weighting. Linear interpolation was used to calculate the concentration of the parent in plasma at the time points of time–activity curves of tissue. The rate constants K_1 and k_2 represent the influx and efflux rates, respectively, for radioligand diffusion across the BBB. For 2-TCM, the rate constants k_3 and k_4 represent radioligand transfer between the compartments for nondisplaceable and specifically bound radioligand, respectively. V_T is equal to the ratio of the concentration of radioligand in tissue to that in plasma at equilibrium. Blood volume was fixed at 0.05 mL/mL (*24*). The binding potential (BP_{ND}) of ^{18}F-FE-PE2I was quantified by the indirect kinetic method. We used the cerebellum as the reference brain region because of its negligible DAT density as shown in a human autoradiographic study (*25*) and an in vivo displacement study in monkeys (*20*). BP_{ND} can be expressed as:

$$BP_{ND} = \left(V_{T(regions)}/V_{T(cerebellum)}\right) - 1,$$

where $V_{T(regions)}$ and $V_{T(cerebellum)}$ are V_T of target regions and the cerebellum, respectively.

Time–Stability Analysis

To investigate the effect of scan length on the estimation of V_T, we analyzed PET data while truncating scan length. The scan length from 90 to 40 min, with 10-min decrements, was analyzed to estimate V_T of varying scan lengths, using the parent concentration in plasma as the input function. For each region and duration,

V_T was expressed as the percentage of the V_T value obtained with a 90-min scan length.

Kinetic Analysis with Radiometabolite-Included Input Function

To assess the effect of lipophilic radiometabolites, we tested an alternative input function consisting of the concentration of the parent and the lipophilic radiometabolite, 4-hydroxymethyl analog of the parent (M1), to estimate rate constants and V_T.

Simplified Reference Tissue Model (SRTM)

^{18}F-FE-PE2I binding was also quantified by the SRTM method with the cerebellum as a reference region. Assuming that both target and reference regions have the same level of nondisplaceable binding, and the kinetics in the target and reference regions can be described by 1-TCM, BP_{ND} is obtained by solving the convolution equation using a nonlinear least-squares fitting procedure (*26*). In this method, the parameters are reduced to 3: R_1 (ratio of K_1 relative to the reference region), k_2, and BP_{ND}. In addition, to investigate the applicability of shorter study durations, BP_{ND} values estimated by the indirect kinetic method and by the SRTM method with 60-min scanning data were compared with those estimated with 90-min scanning data.

Statistical Analysis

The goodness of curve fitting of models with different levels of complexity was compared using the Akaike information criterion (AIC) (*27*) and F test. In a model with better fitting, AIC shows lower values. A P value of less than 0.05 was considered significant for the F test. The SE of kinetic parameters was given by the diagonal of the covariate matrix (*28*). Divided by the estimate of the parameter itself, SE was expressed as a percentage (SE/[estimates of the parameter]) and used to assess parameter identifiability. A smaller percentage indicates better identifiability. Pearson r and linear regression analyses were used to assess correlations between BP_{ND} values estimated with the different approaches. A paired t test was applied to assess the difference in BP_{ND} values between the indirect kinetic and SRTM methods.

RESULTS

Brain Uptake

After the injection of ^{18}F-FE-PE2I, the radioactivity was distributed throughout the brain, with a high peak (~3–5 SUV) and fast washout (Figs. 1 and 2A). The peak uptake occurred within 10 min in all regions. The rank order of radioactivity from approximately 15 min to the end of the scan was as follows: putamen and caudate >> midbrain > thalamus > cerebellum. The uptake in the midbrain was visible as 2 distinct regions. Specific binding, which is the difference in radioactivity between target regions and the cerebellum, reached peak levels within approximately 30 min after injection in all target regions (Fig. 2B). The ratio of radioactivity in the striatum to that in the cerebellum reached a peak level (~7.0) approximately 60 min after the injection and remained at almost the same level thereafter (Fig. 2C).

[Fig. 1] [Fig. 2]

Plasma Analysis

Reversed-phase HPLC analysis of plasma resulted in the separation of the parent and 2 major radiolabeled components (Fig. 3A). The peak with longest retention time corresponded to the parent, representing approximately 14% of plasma radioactivity at 30 min after injection (Fig. 3B). Of the 2 major radiolabeled components, one (M1) was retained longer, representing approximately 20% of plasma radioactivity at 30 min after injection. The M1-to-parent ratio was stable (~1.3–1.4) at 20 min after injection. Retention of the other one (M2) was shorter and consisted of 2 peaks, which were not sufficiently separated from each other, representing approximately 70% of the plasma radioactivity at 30 min after injection. The concentration of the parent showed a quick peak and fast washout in plasma (Fig. 3C).

[Fig. 3]

RGB

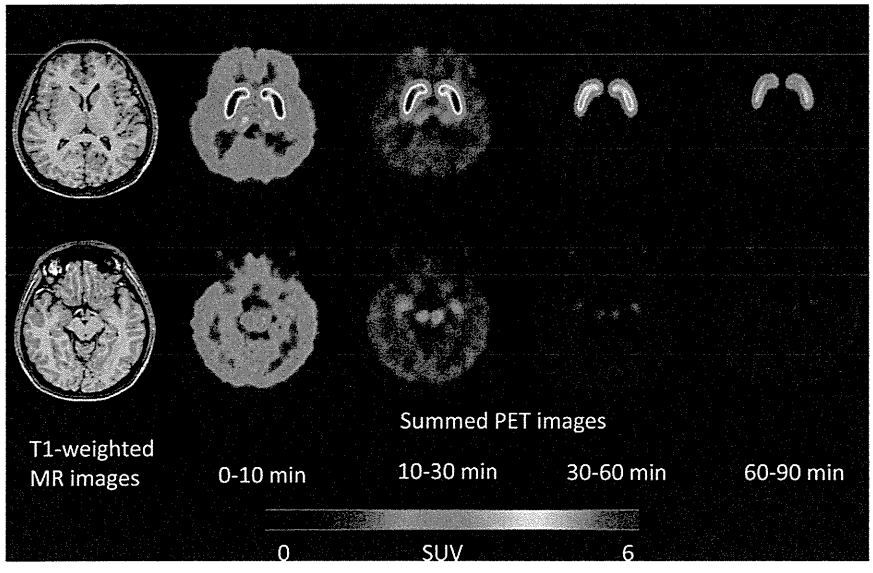

FIGURE 1. Representative dynamic PET images of healthy subject injected with ^{18}F-FE-PE2I. PET images were created at level of striatum (top) and midbrain (bottom). SUV = standardized uptake value.

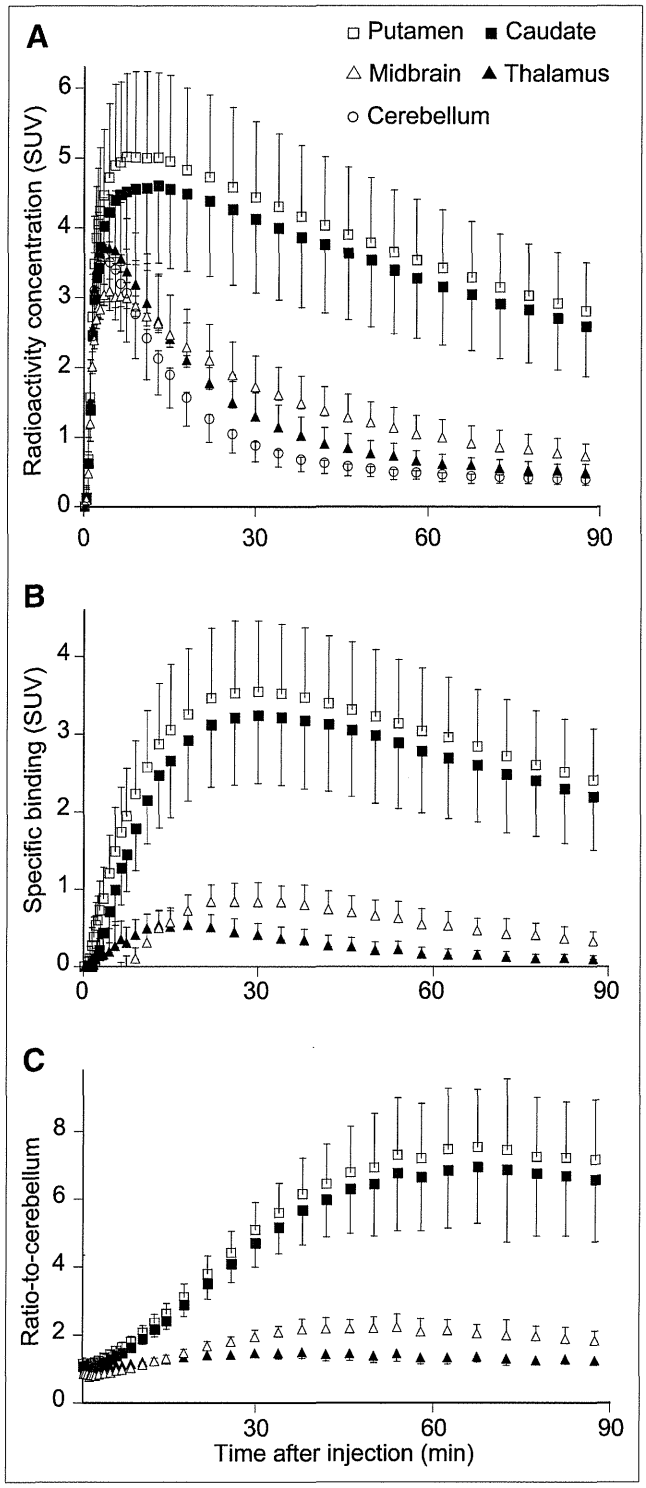

FIGURE 2. Average time course of radioactivity in brain regions after injection of ^{18}F-FE-PE2I. Time course for regional radioactivity (A), specific binding (B), and ratio to cerebellum (C). Data represent mean ± SD of all 10 subjects. SUV = standardized uptake value.

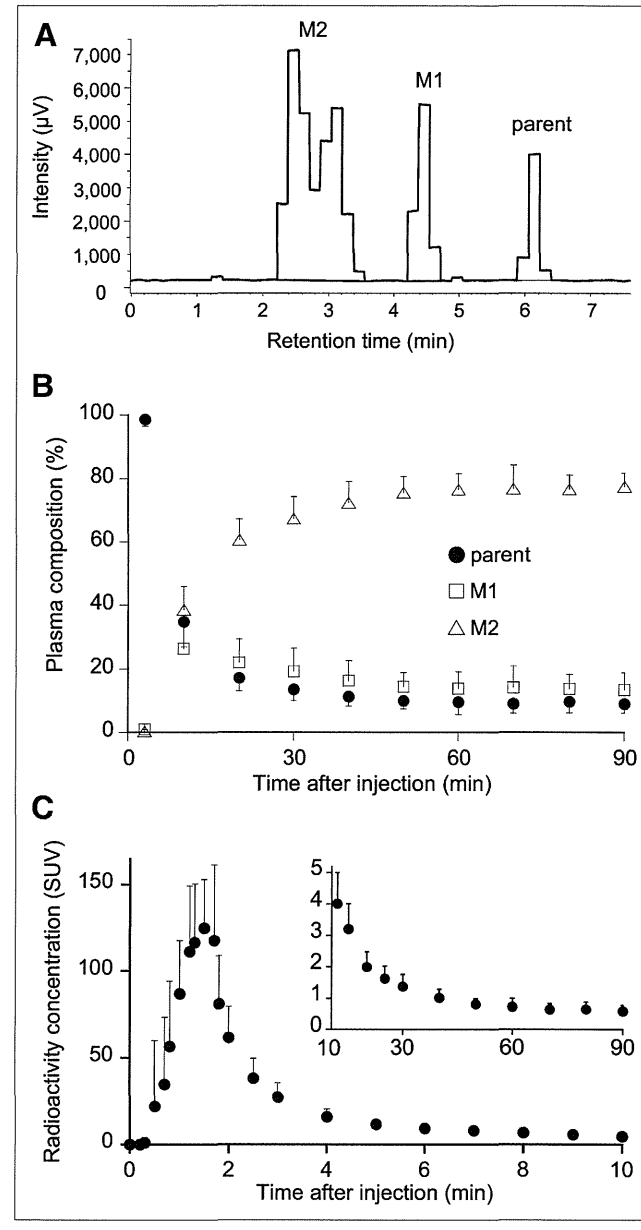

FIGURE 3. Concentration of ^{18}F-FE-PE2I and its composition in arterial plasma after injection of ^{18}F-FE-PE2I. (A) Representative radiochromatogram at 30 min after injection of ^{18}F-FE-PE2I. (B) Plasma composition of parent, M1, and M2. (C) Concentration of ^{18}F-FE-PE2I in plasma. Values from 0 to 10 and 10 to 90 min are shown in each graph with different ranges of *y*-axis. Data represent mean ± SD of all 10 subjects. SUV = standardized uptake value.

Quantification of DAT by Compartment Analysis

The 2-TCM provided significantly better fitting than the 1-TCM for all subjects in all regions. AIC of the 2-TCM was significantly lower than that of the 1-TCM in all regions in all subjects (paired *t* test, $P < 0.05$). The *F* test showed that the 2-TCM gave statistically better fittings than did the 1-TCM in all regions in all subjects ($F > 10.2$, $P < 0.001$). Thus, time–activity curves of all regions including the cerebellum were better described by the 2-TCM (Fig. 4). [Fig. 4]

The 2-TCM estimated K_1 and V_T with good identifiability (1.8% and 3.7%, respectively) (Table 1). BP_{ND} values estimated by the indirect kinetic method were approximately 4.0–4.5 in the putamen and caudate, approximately 0.5 in [Table 1]

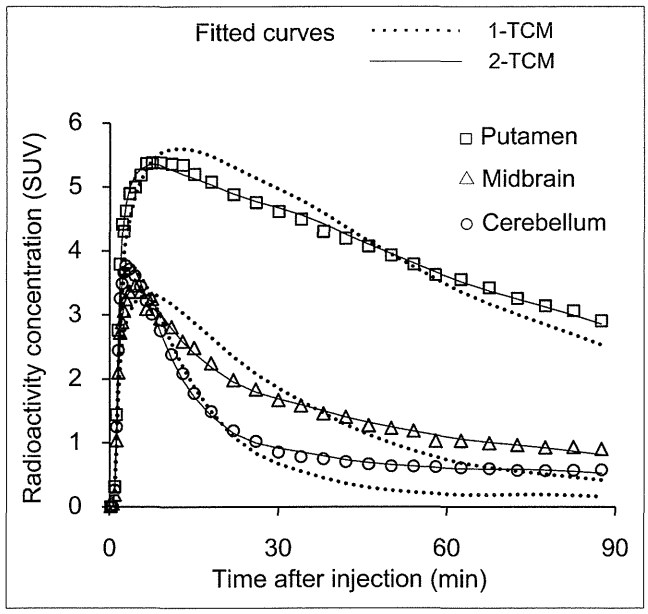

FIGURE 4. Representative fitted model curves of 1-TCM and 2-TCM. Time–activity curves in putamen, midbrain, and cerebellum were fitted to 1-TCM and 2-TCM using parent in plasma as input function. The 2-TCM (solid line) provided better fittings than 1-TCM (dotted line) for all 3 regions. SUV = standardized uptake value.

the midbrain, and approximately 0.2 in the thalamus [Table 2] (Table 2). As to the intersubject variability, the coefficients of variation (100 × SD/mean) of the BP_{ND} values were approximately 20%–25% in the putamen and caudate, approximately 30% in the midbrain, and approximately 60% in the thalamus.

Effects of Scan Length on Quantification of DAT

V_T values were stably estimated using the 2-TCM with 60-min or longer scan length. In the putamen and cerebellum, V_T values gradually increased with longer scan length [Fig. 5] (Figs. 5A and 5B). With a 60-min scan length, V_T values were approximately 94% and 90% of those with full scan length in the putamen and cerebellum, respectively, indicating that V_T values were stably estimated with a 60-min or longer scan length. Identifiability of V_T in the putamen improved over time, reaching approximately 2% at 90 min, whereas in the cerebellum, it remained at almost the same level (~6%) at a 60-min or longer scan length.

Effects of Adding Lipophilic Radiometabolite to Input Function on Quantification of DAT

To assess the effect of the lipophilic radiometabolite, we tested an alternative input function consisting of the concentration of the parent and M1, the lipophilic radiometabolite. Although the 2-TCM showed significantly better fitting than did the 1-TCM in the putamen, caudate, and midbrain based on AIC and the F test, V_T was not well identified by the 2-TCM in the thalamus in some subjects and in the cerebellum in most subjects. In the putamen, caudate, and midbrain, V_T values estimated using the alternative input function were approximately 30%–35% lower than V_T values estimated with the parent concentration in plasma as the input function (Supplemental Table 1; supplemental materials are available online only at http://jnm.snmjournals.org).

Quantification of DAT with SRTM Method

BP_{ND} values estimated by the SRTM method were approximately 3.6–4.0 in the putamen and caudate, approximately 0.6 in the midbrain, and approximately 0.3 in the thalamus (Table 2). Simple correlation analysis showed good correlation between BP_{ND} values estimated by the indirect kinetic method and by the SRTM method (r = 0.990, $P < 0.0001$) (Fig. 6), although there was significant [Fig. 6] difference between these values ($P = 0.0094$, paired t test). A Bland–Altman plot showed that the SRTM method underestimated BP_{ND} in the high-density regions and overestimated BP_{ND} in the low-density regions; however, the magnitude of the bias was small (~10% in the putamen, caudate, and midbrain) (Supplemental Fig. 1). The intersubject variability of BP_{ND} by the SRTM method was

TABLE 1
Kinetic Parameters by 2-TCM Using Parent as Input Function

Region	K_1 (mL·cm^{-3}·min^{-1})	k_2 (min^{-1})	k_3 (min^{-1})	k_4 (min^{-1})	K_1/k_2 (mL·cm^{-3})	k_3/k_4	V_T (mL·cm^{-3})	AIC
Putamen	0.292 ± 0.053 (1.7)	0.073 ± 0.022 (15)	0.133 ± 0.030 (21)	0.043 ± 0.007 (8.6)	4.25 ± 1.07 (13)	3.19 ± 0.97 (17)	17.3 ± 4.6 (2.0)	−43 ± 21
Caudate	0.248 ± 0.047 (1.7)	0.051 ± 0.022 (19)	0.110 ± 0.063 (38)	0.051 ± 0.014 (17)	5.71 ± 2.69 (18)	2.09 ± 0.93 (27)	16.2 ± 5.5 (2.6)	−38 ± 16
Midbrain	0.203 ± 0.044 (2.6)	0.095 ± 0.026 (13)	0.053 ± 0.028 (34)	0.042 ± 0.009 (22)	2.18 ± 0.37 (11)	1.29 ± 0.55 (18)	4.9 ± 1.1 (3.8)	20 ± 20
Thalamus	0.269 ± 0.042 (1.7)	0.123 ± 0.024 (6.0)	0.029 ± 0.018 (26)	0.041 ± 0.023 (23)	2.26 ± 0.55 (4.7)	0.71 ± 0.20 (12)	3.8 ± 0.8 (3.8)	10 ± 16
Cerebellum	0.265 ± 0.031 (1.2)	0.141 ± 0.025 (3.5)	0.013 ± 0.005 (23)	0.023 ± 0.013 (30)	1.94 ± 0.44 (2.6)	0.67 ± 0.32 (15)	3.2 ± 0.7 (6.3)	−4 ± 29

Values are mean ± SD (n = 10), with percentage SE (which is inversely related to identifiability of parameters) in parentheses.

TABLE 2
BP_{ND} Values by Indirect Kinetic and SRTM Methods

Region	BP_{ND}	
	Indirect kinetic	SRTM
Putamen	4.46 ± 0.95	4.05 ± 0.66
Caudate	4.06 ± 1.04	3.61 ± 0.67
Midbrain	0.55 ± 0.17	0.62 ± 0.13
Thalamus	0.20 ± 0.12	0.29 ± 0.08

Values are mean ± SD (n = 10).

approximately 15%–20% in the striatum and midbrain and approximately 30% in the thalamus, which were overall smaller than those by the indirect kinetic method. When BP_{ND} values estimated by the indirect kinetic method and by the SRTM method with 60-min data were compared with those estimated with 90-min data, good correlations were observed (r = 0.992 for the indirect kinetic method and 0.999 for the SRTM method, $P < 0.0001$ for both, Figs. 7A and 7B).

[Fig. 7]

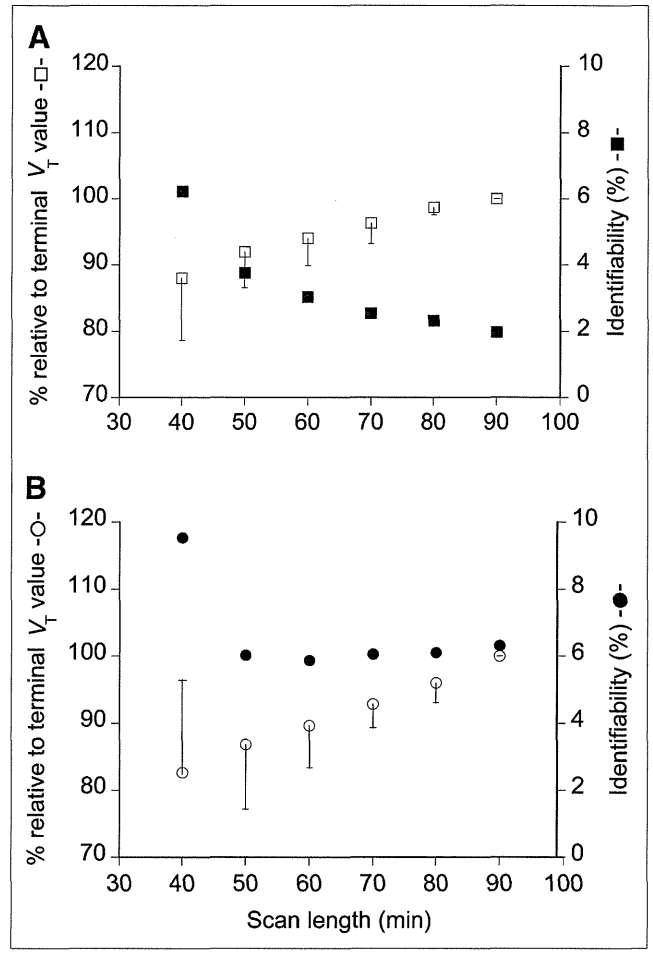

FIGURE 5. Value of V_T and identifiability as function of scan length. V_T and its corresponding SE (%) (SE (%)) were estimated in putamen (A) and cerebellum (B) with 2-TCM using parent as input function with truncating scan length from 90 to 40 min. V_T values are expressed as percentage of terminal value and plotted along left y-axis for putamen (□) and cerebellum (○). Corresponding SE (%), which is inversely related to identifiability, is plotted along right y-axis for putamen (■) and cerebellum (●). Error bar represents SD (n = 10).

DISCUSSION

^{18}F-FE-PE2I is a promising radioligand for quantifying DAT in healthy humans. The kinetics of ^{18}F-FE-PE2I were well described by a standard 2-TCM using the parent radioligand in plasma as the input function. Although the radiometabolites of ^{18}F-FE-PE2I possibly have some effect on the radioactivity in the brain, the effect on the quantification was likely to be small. As a noninvasive quantification of DAT, the SRTM method was validated. The quantification was stable in both the striatum and the midbrain for both the indirect kinetic method with 2-TCM and the SRTM method with a scan duration of 60 min.

General kinetics of ^{18}F-FE-PE2I showed promising characteristics, including a high specific-to-nonspecific ratio and relatively fast washout. Uptake was high in the putamen and caudate, relatively low in the midbrain and thalamus, and lowest in the cerebellum. In all target regions, specific binding reached maximum values within the duration of PET data acquisition, and transient equilibrium was reached during this acquisition period. Uptake in the midbrain was visualized as 2 distinct regions. Given the selectivity of ^{18}F-FE-PE2I for DAT in the midbrain shown by a displacement study (*20*), we suppose that this uptake reflected DAT binding, not serotonin transporter binding.

Compartment model analysis showed that the kinetics of ^{18}F-FE-PE2I were well described by the 2-TCM using the parent radioligand in plasma as the input function. To estimate BP_{ND}, we applied the indirect kinetic method instead of directly using the ratio of k_3/k_4 values. The k_3/k_4 ratio theoretically equals BP_{ND}, but this estimate tends to be inaccurate because of data noise (*29*). We actually observed that these values showed poor identifiability and were not so reliably estimated (Table 1). Regional BP_{ND} values were in accordance with previous autoradiographic (*25*) and in vivo studies (*16,17*). As to intersubject variability, coefficients of variation of the BP_{ND} values were good in the putamen and caudate, acceptable in the midbrain, and poor in the thalamus. Because the BP_{ND} value in the midbrain was low (~13% of that in the striatum) in comparison with the results of autoradiography (~50% of that in the striatum) (*25*), the BP_{ND} values in the midbrain could be affected by the partial-volume effect. Similar results were obtained in nonhuman primates using high-resolution research tomography. BP_{ND} in the midbrain was approximately 15% of the values in the striatum (*21*).

Although radiometabolites of ^{18}F-FE-PE2I possibly have some effects on radioactivity in the brain, their effect on quantification was likely to be small. HPLC analysis detected 2 radiometabolites of ^{18}F-FE-PE2I in plasma,

jnm101626-pm ■ 6/11/12

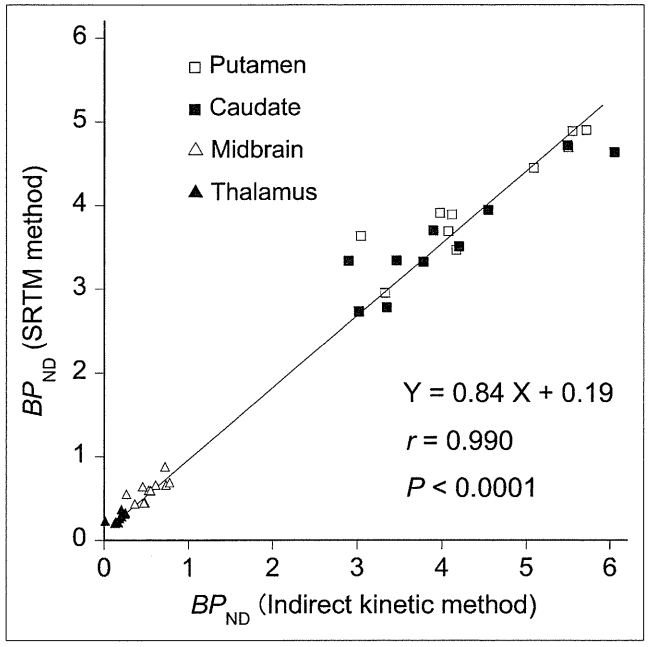

FIGURE 6. Correlation of BP_{ND} values estimated by indirect kinetic method using parent as input function and by SRTM method. BP_{ND} values showed significant correlation between 2 methods. Each data point represents BP_{ND} values in respective regions of each subject.

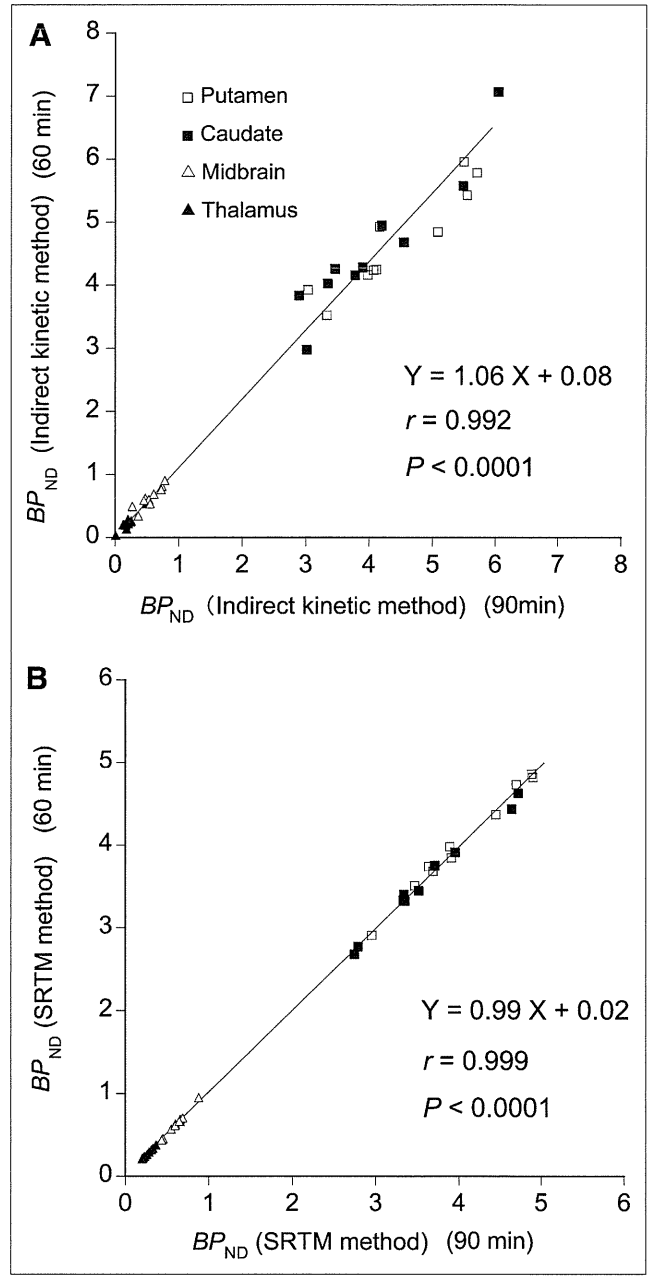

FIGURE 7. Correlation of BP_{ND} values estimated with 60- and 90-min data. (A) BP_{ND} values estimated by indirect kinetic method. (B) BP_{ND} values estimated by SRTM method. Significant correlations were observed in both methods between estimates with 60- and 90-min data.

one with intermediate (M1) and the other with lower (M2) lipophilicity. M1 and M2 would be 4-hydroxymethyl and 4-carboxyl analogs of ^{18}F-FE-PE2I, respectively, on the basis of the retention time of HPLC analysis, compared with the rat study (*19*). For clarity, in the following sentences, we refer to 4-hydroxymethyl and 4-carboxyl analogs of ^{11}C-PE2I as M1′ and M2′, respectively. In rats, M1′ entered the brain, accumulated in the striatum to a lesser extent than ^{11}C-PE2I, and metabolized to M2′, which accumulated in the brain. Mainly as a result of the accumulation of M2′, radioactivity in the cerebellum of rats did not decrease from 55 min to the end of the scan (120 min) (*19*). Whereas in the current study with ^{18}F-FE-PE2I, radioactivity in the cerebellum showed a gradual decrease to the end of the scan (90 min) (Fig. 2A), indicating that the amount of retention of radiometabolites in the brain in humans with ^{18}F-FE-PE2I was less than that in rats with ^{11}C-PE2I. This result was in accordance with the study in monkeys with ^{18}F-FE-PE2I (*21*).

The effects of radiometabolites on the quantification were small in the target and reference regions. To evaluate the effect of the possible accumulation of radiometabolites on the estimation of V_T, we performed a time–stability analysis of V_T. The increase in V_T with an increase in scan length could be interpreted as evidence for the accumulation of radiometabolites in the brain (*30*). In the current study, V_T values by the 2-TCM in the putamen and cerebellum with 60-min data were approximately 94% and 90% of terminal values with 90-min data (Fig. 6). This finding might indicate that V_T values were slightly affected by the radiometabolites, but the effects were relatively small.

To estimate the possible bias by the radiometabolites on V_T, we tried a combined input function of the parent and the radiometabolite M1 as previously performed by Varrone et al. in nonhuman primates using^{18} F-FE-PE2I (*21*). The main assumption of this approach is that the parent and the radiometabolite M1 would behave similarly and hence could be combined in a single input. With this approach,

the 2-TCM yielded approximately 30%–35% lower estimates of V_T values in the striatum and midbrain than with the 2-TCM using the parent as the input function. The decrease of V_T could be a possible maximum bias by the radiometabolites. However, the V_T values estimated by the 2-TCM using a summation of the parent and M1 as the input function were not well identified in some subjects in the thalamus and in most in the cerebellum. Because combining the parent and M1 as the input function did not improve the fitting, at least for these regions the assumption was not fully supported by the data. Identification of the radiometabolites of ^{18}F-FE-PE2I and assessment of their affinity for the DAT would be necessary to confirm or rule out the above assumption.

As a less noninvasive quantification of DAT without arterial blood data, BP_{ND} values were well estimated by the SRTM method using the cerebellum as the reference region. BP_{ND} values estimated by the SRTM method were well correlated with those estimated by the indirect kinetic method with the 2-TCM, which was not so much affected by radiometabolites as we discussed above. The SRTM method yielded slight underestimation and overestimation of BP_{ND} values in regions with high and low DAT densities, respectively, although the magnitude of the bias was small (~10% in the putamen, caudate, and midbrain). This bias seems to be an intrinsic limitation of the SRTM method because a similar phenomenon was observed in other ligands, including the serotonin 5-hydroxytryptamine-1A ligand ^{11}C-WAY-100653 (*31*), perhaps because of a violation of the assumptions of SRTM method. The intersubject variability of BP_{ND} values by the SRTM method were better than those by the indirect kinetic method with the 2-TCM, indicating that the SRTM method provided more precise estimation of BP_{ND} in all regions, including the midbrain.

Time–stability analysis indicated that 60-min scan duration is enough to estimate DAT binding with ^{18}F-FE-PE2I in humans. A recent study in nonhuman primates indicated that an approximately 60-min scan length was sufficient for the quantification of DAT with ^{18}F-FE-PE2I by the SRTM method (*32*). In the current study in humans, quantification was stable for both the indirect kinetic method and SRTM method with a scan duration of 60 min. Good correlations were observed between BP_{ND} values estimated with 60- and 90-min data for both the indirect kinetic method and the SRTM method.

^{18}F-FE-PE2I has many desirable characteristics among DAT ligands available for human imaging. High affinity and high selectivity for DAT allowed reliable quantification of specific binding not only in the striatum but also in the midbrain. Because of the faster kinetics even in high-density regions (i.e., the striatum), quantification with a shorter time (60 min) was possible, and the SRTM method yielded less biased BP_{ND} in the striatum than ^{11}C-PE2I. In addition, labeling with ^{18}F, which has a longer half-life than ^{11}C (110 vs. 20 min), allows distribution of the radioligand to PET centers without a cyclotron.

^{18}F-labeled DAT ligands previously reported in humans include ^{18}F-FPCIT (*12*), ^{18}F-CFT (^{18}F-WIN35,428) (*11*), and ^{18}F-FECNT (*13*). All of these ligands have a high affinity for DAT, and the maximum striatum-to-cerebellum ratios have been reported to be approximately 3.5–9.0. The possible advantage of ^{18}F-FPCIT and ^{18}F-FECNT could be the absence of potentially BBB-permeable radiometabolites. However, the disadvantage of those ligands was that the kinetics are slow, requiring over 90 min to reach peak brain uptake in the striatum. Among ^{18}F-labeled DAT ligands, ^{18}F-FE-PE2I has a relatively high striatum-to-cerebellum ratio (~7.0) and obviously the fastest kinetics.

One of the 2 limitations of the current study is the absence of the measurement of the free fraction in plasma, which would enable us to measure DAT density more accurately. Another limitation is the absence of an animal ex vivo study using ^{18}F-FE-PE2I to examine the BBB permeability and affinity for DAT of the radiometabolites. These issues should be explored in future studies.

CONCLUSION

^{18}F-FE-PE2I is a promising radioligand for quantifying DAT in healthy humans. The kinetics of ^{18}F-FE-PE2I were well described by a standard 2-TCM using the parent radioligand in plasma as the input function. Although radiometabolites of ^{18}F-FE-PE2I possibly have some effect on the radioactivity in the brain, their effect on quantification was likely to be small. As a noninvasive quantification of DAT, the SRTM method was validated. The quantification was stable in both the striatum and the midbrain for both the indirect kinetic method with 2-TCM and the SRTM method with a scan duration of 60 min, although the SRTM method yielded a slight underestimation and overestimation of BP_{ND} values in regions with high and low DAT densities, respectively. If no major differences in metabolism between patients and controls are present in clinical studies, noninvasive estimation of BP_{ND} by the SRTM method with a 60-min scan will be sufficiently accurate for DAT quantification.

DISCLOSURE STATEMENT

The costs of publication of this article were defrayed in part by the payment of page charges. Therefore, and solely to indicate this fact, this article is hereby marked "advertisement" in accordance with 18 USC section 1734.

ACKNOWLEDGMENTS

We thank Katsuyuki Tanimoto, Takahiro Shiraishi, and Takehito Ito for their assistance in performing PET experiments and Izumi Izumida and Kazuko Suzuki for their help as clinical research coordinators. This study was supported by a grant-in-aid for Molecular Imaging Program from the Ministry of Education, Culture, Sports, Science and Technology and by a Health Labour Sciences Research

grant from the Ministry of Health, Labour and Welfare, Japanese government. No other potential conflict of interest relevant to this article was reported.

REFERENCES

1. Hurley MJ, Mash DC, Jenner P. Markers for dopaminergic neurotransmission in the cerebellum in normal individuals and patients with Parkinson's disease examined by RT-PCR. *Eur J Neurosci.* 2003;18:2668–2672.
2. Ginovart N, Lundin A, Farde L, et al. PET study of the pre- and post-synaptic dopaminergic markers for the neurodegenerative process in Huntington's disease. *Brain.* 1997;120:503–514.
3. Jucaite A, Fernell E, Halldin C, Forssberg H, Farde L. Reduced midbrain dopamine transporter binding in male adolescents with attention-deficit/hyperactivity disorder: association between striatal dopamine markers and motor hyperactivity. *Biol Psychiatry.* 2005;57:229–238.
4. Nakamura K, Sekine Y, Ouchi Y, et al. Brain serotonin and dopamine transporter bindings in adults with high-functioning autism. *Arch Gen Psychiatry.* 2010;67:59–68.
5. Arakawa R, Ichimiya T, Ito H, et al. Increase in thalamic binding of [^{11}C]PE2I in patients with schizophrenia: a positron emission tomography study of dopamine transporter. *J Psychiatr Res.* 2009;43:1219–1223.
6. Fowler JS, Volkow ND, Wolf AP, et al. Mapping cocaine binding sites in human and baboon brain in vivo. *Synapse.* 1989;4:371–377.
7. Wong DF, Yung B, Dannals RF, et al. In vivo imaging of baboon and human dopamine transporters by positron emission tomography using [^{11}C]WIN 35,428. *Synapse.* 1993;15:130–142.
8. Farde L, Halldin C, Muller L, Suhara T, Karlsson P, Hall H. PET study of [^{11}C] beta-CIT binding to monoamine transporters in the monkey and human brain. *Synapse.* 1994;16:93–103.
9. Ding YS, Fowler JS, Volkow ND, et al. Pharmacokinetics and in vivo specificity of [^{11}C]dl-threo-methylphenidate for the presynaptic dopaminergic neuron. *Synapse.* 1994;18:152–160.
10. Fischman AJ, Bonab AA, Babich JW, et al. [^{11}C, ^{127}I] Altropane: a highly selective ligand for PET imaging of dopamine transporter sites. *Synapse.* 2001;39:332–342.
11. Laakso A, Bergman J, Haaparanta M, Vilkman H, Solin O, Hietala J. [^{18}F]CFT ([^{18}F]WIN 35,428], a radioligand to study the dopamine transporter with PET: characterization in human subjects. *Synapse.* 1998;28:244–250.
12. Kazumata K, Dhawan V, Chaly T, et al. Dopamine transporter imaging with fluorine-18-FPCIT and PET. *J Nucl Med.* 1998;39:1521–1530.
13. Davis MR, Votaw JR, Bremner JD, et al. Initial human PET imaging studies with the dopamine transporter ligand ^{18}F-FECNT. *J Nucl Med.* 2003;44:855–861.
14. Emond P, Garreau L, Chalon S, et al. Synthesis and ligand binding of nortropane derivatives: N-substituted 2beta-carbomethoxy-3beta-(4′-iodophenyl)nortropane and N-(3-iodoprop-(2E)-enyl)-2beta-carbomethoxy-3beta-(3′,4′-disubstituted phenyl)nortropane: new high-affinity and selective compounds for the dopamine transporter. *J Med Chem.* 1997;40:1366–1372.
15. Halldin C, Erixon-Lindroth N, Pauli S, et al. [^{11}C]PE2I: a highly selective radioligand for PET examination of the dopamine transporter in monkey and human brain. *Eur J Nucl Med Mol Imaging.* 2003;30:1220–1230.
16. Jucaite A, Odano I, Olsson H, Pauli S, Halldin C, Farde L. Quantitative analyses of regional [^{11}C]PE2I binding to the dopamine transporter in the human brain: a PET study. *Eur J Nucl Med Mol Imaging.* 2006;33:657–668.
17. Hirvonen J, Johansson J, Teras M, et al. Measurement of striatal and extrastriatal dopamine transporter binding with high-resolution PET and [^{11}C]PE2I: quantitative modeling and test-retest reproducibility. *J Cereb Blood Flow Metab.* 2008;28:1059–1069.
18. Seki C, Ito H, Ichimiya T, et al. Quantitative analysis of dopamine transporters in human brain using [^{11}C]PE2I and positron emission tomography: evaluation of reference tissue models. *Ann Nucl Med.* 2010;24:249–260.
19. Shetty HU, Zoghbi SS, Liow JS, et al. Identification and regional distribution in rat brain of radiometabolites of the dopamine transporter PET radioligand [^{11}C] PE2I. *Eur J Nucl Med Mol Imaging.* 2007;34:667–678.
20. Varrone A, Steiger C, Schou M, et al. In vitro autoradiography and in vivo evaluation in cynomolgus monkey of [^{18}F]FE-PE2I, a new dopamine transporter PET radioligand. *Synapse.* 2009;63:871–880.
21. Varrone A, Toth M, Steiger C, et al. Kinetic analysis and quantification of the dopamine transporter in the nonhuman primate brain with ^{11}C-PE2I and ^{18}F-FE-PE2I. *J Nucl Med.* 2011;52:132–139.
22. Schou M, Steiger C, Varrone A, Guilloteau D, Halldin C. Synthesis, radiolabeling and preliminary in vivo evaluation of [^{18}F]FE-PE2I, a new probe for the dopamine transporter. *Bioorg Med Chem Lett.* 2009;19:4843–4845.
23. Innis RB, Cunningham VJ, Delforge J, et al. Consensus nomenclature for in vivo imaging of reversibly binding radioligands. *J Cereb Blood Flow Metab.* 2007;27: 1533–1539.
24. Leenders KL, Perani D, Lammertsma AA, et al. Cerebral blood flow, blood volume and oxygen utilization: normal values and effect of age. *Brain.* 1990; 113:27–47.
25. Hall H, Halldin C, Guilloteau D, et al. Visualization of the dopamine transporter in the human brain postmortem with the new selective ligand [^{125}I]PE2I. *Neuroimage.* 1999;9:108–116.
26. Lammertsma AA, Hume SP. Simplified reference tissue model for PET receptor studies. *Neuroimage.* 1996;4:153–158.
27. Akaike H. A new look at the statistical model identification. *IEEE Trans Automat Contr.* 1974;19:716–723.
28. Carson R. Parameters estimation in positron emission tomography. In: Phelps M, Mazziotta J, Schelbert H, eds. *Positron Emission Tomography Principle Applications for the Brain and the Heart.* New York, NY: Raven Press; 1986:347–390.
29. Seneca N, Skinbjerg M, Zoghbi SS, et al. Kinetic brain analysis and whole-body imaging in monkey of [^{11}C]MNPA: a dopamine agonist radioligand. *Synapse.* 2008;62:700–709.
30. Terry G, Liow JS, Chernet E, et al. Positron emission tomography imaging using an inverse agonist radioligand to assess cannabinoid CB1 receptors in rodents. *Neuroimage.* 2008;41:690–698.
31. Parsey RV, Slifstein M, Hwang DR, et al. Validation and reproducibility of measurement of 5-HT1A receptor parameters with [carbonyl-^{11}C]WAY-100635 in humans: comparison of arterial and reference tisssue input functions. *J Cereb Blood Flow Metab.* 2000;20:1111–1133.
32. Varrone A, Gulyas B, Takano A, Stabin MG, Jonsson C, Halldin C. Simplified quantification and whole-body distribution of [^{18}F]FE-PE2I in nonhuman primates: prediction for human studies. *Nucl Med Biol.* 2012;39:295–303.

Journal of Chromatography B, 879 (2011) 3169–3183

Contents lists available at SciVerse ScienceDirect

Journal of Chromatography B

journal homepage: www.elsevier.com/locate/chromb

Review

Analysis of free D-serine in mammals and its biological relevance☆

Toru Nishikawa*

Department of Psychiatry and Behavioral Sciences, Graduate School of Medical and Dental Sciences, Tokyo Medical and Dental University, 1-5-45, Yushima, Bunkyo-ku, Tokyo 113-8519, Japan

ARTICLE INFO

Article history:
Received 8 April 2011
Accepted 24 August 2011
Available online 30 August 2011

Keywords:
Brain
D-Serine
N-methyl-D-aspartate receptor
Glutamate neurotransmission
Neuropsychiatric disorders
Synapse–glia interaction

ABSTRACT

D-Serine is a unique endogenous substance enriched in the brain at the exceptionally high concentrations as a free D-amino acid in mammals throughout their life. Peripheral tissues and blood contain low or trace levels of the D-amino acid. In the nervous systems, D-serine appears to act as an intrinsic coagonist for the *N*-methyl-D-aspartate type glutamate receptor (NMDA receptor) based upon the following characteristics: (i) D-serine stereoselectively binds to and stimulates the glycine-regulatory site of the NMDA receptor consisting of GRIN1/GRIN2 subunits more potently than glycine with an affinity and ED50 at high nanomolar ranges, (ii) the selective elimination of D-serine in brain tissues attenuates the NMDA receptor functions, indicating an indispensable role in physiological activation of the glutamate receptor, and (iii) the distribution of D-serine is uneven and closely correlated with that of the binding densities of the various NMDA receptor sites, and especially of the GRIN2B subunit in the brain. Moreover, D-serine exerts substantial influence on the GRIN1/GRIN3-NMDA and δ2 glutamate receptor. In the brain and retina, metabolic processes of D-serine, such as biosynthesis, extracellular release, uptake, and degradation, are observed and some candidate molecules that mediate these processes have been isolated. The fact that the mode of extracellular release of D-serine in the brain differs from that of classical neurotransmitters is likely to be related to the detection of D-serine in both glial cells and neurons, suggesting that D-serine signals could be required for the glia–synapse interaction. Moreover, the findings from the basic experiments and clinical observations support the views that the signaling system of endogenous free D-serine plays important roles, at least, through the action on the NMDA receptors in the brain wiring development and the regulation of higher brain functions, including cognitive, emotional and sensorimotor function. Based upon these data, aberrant D-serine–NMDA receptor interactions have been considered to be involved in the pathophysiology of a variety of neuropsychiatric disorders including schizophrenia and ischemic neuronal cell death. The molecular and cellular mechanisms for regulating the D-serine signals in the nervous system are, therefore, suitable targets for studies aiming to elucidate the causes of neuropsychiatric disorders and for the development of new treatments for intractable neuropsychiatric symptoms.

Contents

Abbreviations: Aβ, amyloid β peptide; ALS, amyotrophic lateral sclerosis; AMPA, α-amino-3-hydroxy-5-methyl-4-isoxazolepropionic acid; Asc-1, Na^+-independent alanine–serine–cysteine transporter 1; ASCT2, Na^+-dependent broad-spectrum neutral amino acid transporter 2; BBB, blood–brain barrier; CBT, cognitive behavioral therapy; CNS, central nervous system; DAO, D-amino acid oxidase; DAOA, D-amino acid oxidase activator; DA, dopamine; DPAG, dorsal periaqueductal gray matter; D-ser, D-serine; Dsm-1/PAPST-1, D-serine modulator-1/3′-phosphoadenocine 5′-phosphosulfate transporter-1; GABA, γ-aminobutyric acid; GCS, glycine cleavage system; Gly, glycine; GLYT, glycine transporter; GRIP, glutamate receptor interacting protein; L-glu, L-glutamate; NMDA, *N*-methyl-D-aspartate; 3-PGDH, 3-phosphoglycerate dehydrogenase; PSAT, phosphoserine aminotransferase; PSPH, phosphoserine phosphatase; PTSD, post-traumatic stress disorder; SHMT, serine hydroxymethyltransferase; SNARE, soluble *N*-methylmaleimide susceptibility factor attachment protein receptor; SNP, single nucleotide polymorphisms; SOD1, superoxide dismutase 1; SRR, serine racemase; THF, tetrahydrofolate.

☆ This paper is part of the special issue "Analysis and biological relevance of D-amino acids and related compounds", Kenji Hamase (Guest Editor).

* Tel.: +81 3 5803 5237; fax: +81 3 5803 0245.
E-mail address: tnis.psyc@tmd.ac.jp

1570-0232/$ – see front matter © 2011 Published by Elsevier B.V.
doi:10.1016/j.jchromb.2011.08.030

1. Introduction – detection of endogenous D-serine in mammals

Prior to the 1990s, D-serine, like the other D-amino acids, had long been believed to be absent in mammalian tissues even though the L-type homo-chirality hypothesis for the amino acids in the organisms had been challenged by the following facts; (a) the occurrence of D-amino acid oxidase in the organisms, including mammals, was identified in 1935 [1], and since then this observation has suggested the existence of the endogenous D-amino acids that serve as the substrates for the enzyme [1], (b) the D-aspartate residues had already been proved in the long-living proteins such as crystalline in mammalian eyes [2], (c) the presence of incorporated or free D-serine had also been reported in the cell wall of bacteria [3], and in silkworm [4–6] and earthworm tissues [7–10] and (d) the transient presence of substantial amounts of free D-aspartate and high ratios with respect to the L-enantiomer had been demonstrated in the mammalian brain and peripheral tissues during the early stage of postnatal development [11]. In the early 1990s, the present author with coworkers at the National Institute of Neuroscience (Japan) discovered by gas chromatography (GC) and GC with mass spectrometry (GC–MS) that free D-serine is present and enriched in the brain at a high concentration comparable with those of classical neurotransmitters and at a large ratio to the L-serine content over the lifetime in the rat [12], under way of the present author's research project exploring new therapies for intractable schizophrenia [13], innovating in the biological significance of D-amino acid. In parallel, Nagata and collaborators [14] revealed using two-dimensional thin-layer chromatography in combination with high-performance liquid chromatography (HPLC) that free D-serine naturally occurs at low levels in the mammalian periphery including the blood and kidney, while studying D-amino acids and D-amino acid oxidase. These pioneering investigations of D-serine carefully exclude the possibility that D-serine is chiefly produced by the enteric bacteria or by the non-enzymatic racemization of L-serine during the assay procedures [12,14]. This review will begin with a brief introduction of the background of the present author's research leading to the detection of brain D-serine as this step in the history of D-serine research was important for gaining an understanding of the physiological functions of D-serine and their association with neuropsychiatric disorders.

One serious and persistent problem in clinical psychiatry is that sufficient social rehabilitation is precluded by symptoms resistant to pharmacotherapy, as is commonly seen in patients with schizophrenia [13,15]. To obtain a clue for a strategy to solve the problem, the present author has paid particular attention to an anesthetic phencyclidine (PCP), which causes schizophrenia-like symptoms that are both responsive and resistant to antipsychotics, a currently available class of drugs for the treatment of schizophrenia [13,15]. In 1983, PCP was found to be a potent non-competitive antagonist for the *N*-methyl-D-aspartate (NMDA)-type glutamate receptor (NMDA receptor) [16]. In the mid-1980s, this author started investigating a comprehensive treatment strategy for treatment-resistant schizophrenia, which facilitates NMDA receptor functions [13,15,17,18], albeit not via the glutamate site agonists that often bring about cell death or convulsions, but rather via the glycine-site stimulators which are unlikely to have such harmful effects [13,15,19].

To this end, the two D-amino acids, D-serine, and D-alanine, were chosen for further investigation for the following reasons: D-serine, and D-alanine, but not glycine itself, show a site- and stereo-selective actions on the NMDA receptor glycine site in that they have a much higher affinity for the NMDA glycine site than the corresponding L-amino acids, and they have very low affinity for the inhibitory glycine receptor [13,15]. According to this author's idea to overcome the poor ability of these polar D-amino acids to cross the blood–brain barrier (BBB) that their lipid-modified compounds could more easily permeate the BBB and thus would serve as a more useful prototypes for the future clinical systemic application, Hidehiko Hibino, Ph.D. at Nippon Oil and Fats, Co. Ltd., invented and supplied the materials, *N*-myristoyl-D-serine and *N*-myristoyl-D-alanine, for our experiments [20]. Our rat studies demonstrated that not only the intracerebroventiricular injection of D-serine and D-alanine [21] but also the systemic administration of their myristoylated compounds antagonized the PCP-induced abnormal behavior, an animal model of antipsychotic-resistant schizophrenia

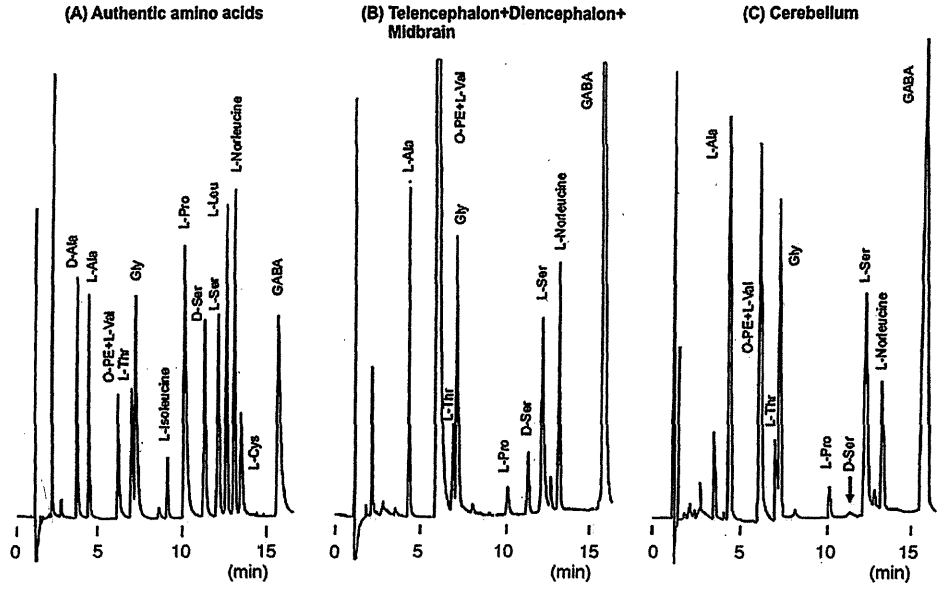

Fig. 1. Gas chromatographic detection of endogenous D-serine in the mammalian brain. The present schemes show representative gas chromatograms of *N,O*-pentafluoropropionyl isopropyl derivatives of the authentic standard amino acids (A), the free amino acids in the extracts of the brain tissues consisting of the telencephalon, diencephalon and midbrain (B) and in those of the cerebellum (C) (unpublished data) in the young adult rats. These gas chromatography assays were performed on a capilally column of Chirasil-L-Val (25 m × 0.25 mm, film thickness 0.12 μm, Gaskuro Kogyo, Japan) as described in Ref. [12]. Note the marked differences in the heights of the D-serine (D-Ser) peaks between the rostral brain regions (B) and the cerebellum (C). L-Norleusine was added as the internal standard. The panels (A) and (B) have been reorganized from the figure published in Ref. [12]. Abbreviations: D-Ala, D-alanine; L-Ala, L-alanine; L-Cys, L-cystein; Gly, glycine; L-Leu, L-leucine; O-PE, O-phosphoethanolamine; L-Pro, L-proline; D-Ser, D-serine; L-Ser, L-serine; L-Thr, L-threonine; L-Val, L-valine.

[20]. This anti-PCP action was barely observed with the corresponding L-forms [21] and attenuated by a selective antagonist for the glycine site [20], supporting the potentiality of an agonist for the NMDA receptor glycine regulatory site as a new antipsychotic.

Furthermore, the present author planned and initiated a study on the possible presence of free D-serine or D-alanine in the brain of rats treated with their myristoylated compounds by GC–MS and HPLC in collaboration with the late Tokishi Hayashi, Ph.D. at the National Institute of Neuroscience to verify the mechanisms of the anti-PCP action of these compounds. By the additional collaboration with Noriko Fujii, Ph.D. at Tsukuba University, we provided the first evidence using GC and GC–MS for the constant presence of D-serine at a substantial content in the rat brain [12]. As this author predicted on the basis of the brain-preferring distribution of D-serine, brain endogenous D-serine was shown to exhibit an NMDA receptor-related distribution [15,22]. From the neuroanatomical and functional correlates of D-serine with the NMDA receptor [15,22] and the presumed anti-schizophrenia action [20,21,23], it was proposed by the present author that brain D-serine might play an important role as an endogenous NMDA receptor allosteric agonist in the regulation of higher brain functions [12,15,22]. After early confirmations of our initial findings were obtained by our group [24–26] and others [27–29], subsequent studies of endogenous D-serine in the central nervous system have expanded to include a wide variety of topics [30].

This review article summarizes the findings regarding the metabolism and function of endogenous D-serine as primarily related to the mammalian brain. The significance of these findings will be discussed in terms of the pathophysiology and the development of novel therapies for neuropsychiatric disorders.

2. Distribution and metabolism of D-serine

Recent advances in the separation and detection techniques for the chiral amino acids have enabled us (the investigators) to perform the qualitative and quantitative examinations of the free or protein-conjugated D-amino acids in the biological samples. Detection of endogenous free D-serine indeed appears to be one of their important products that open a novel path to understand, at least, the complex regulatory systems for the mammalian brain.

2.1. Analysis of free D-serine in mammals

Presently, D-serine can be identified or quantitatively assayed by GC [12] (Fig. 1), GC–MS [12,15], HPLC with fluorometric detection [22,24,31,32] (Fig. 2), thin-layer chromatography in combination with HPLC [14], enzymatic assay using D-serine dehydratase [33], online microdialysis–capillary electrophoresis [34], and immunohistochemical staining by using anti-D-serine antibody raised against protein-conjugated D-serine by glutaraldehyde [29,35–37]. By means of these various methodologies, tissue and cellular localizations and their dynamics of D-serine have extensively been examined (Figs. 3 and 4). Although most investigations on mammalian intrinsic D-serine have focused on the brain, it is also intensively studied in other organs such as spinal cord [26,38], retina [39,40], kidney [14], bone [41], and urine [42]. In these studies, biochemical phenomena that suggest the existence of metabolic and functional processes of D-serine, including biosynthesis, storage, release into extracellular fluid, interaction with the receptor site, uptake, and degradation, are observed (Fig. 5).

2.2. Distribution (Figs. 3 and 4)

In the maturation period of mammals, including rats, mice, and humans, D-serine shows a selective distribution in the brain and retina; its concentration is very low in the spinal cord, peripheral tissues such as kidney and liver, and blood (Fig. 3), but relatively high in the urine (contents in the human urine (18–55 years old), 0.08–0.246 μmol/ml; D-serine to total serine ratios, 18–53%: rat, ratios, 13%) [12,15,22,42]. The distribution in the brain is also uneven; the concentrations of D-serine and

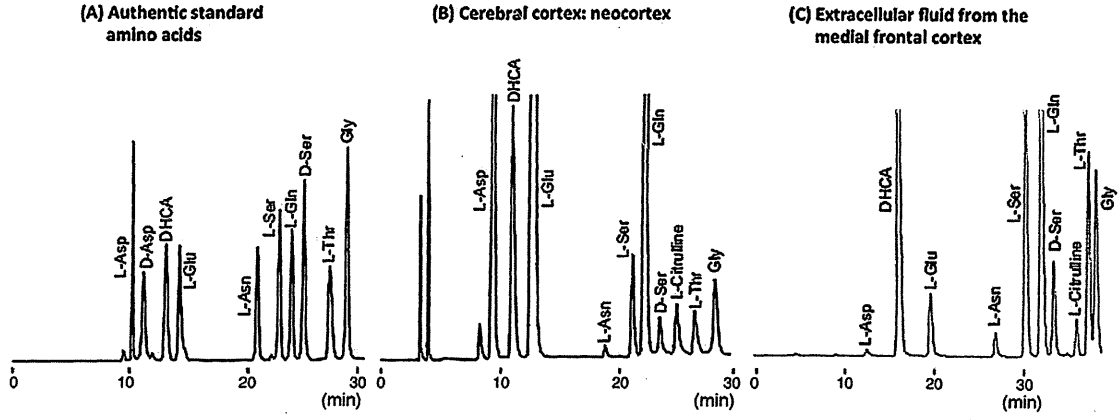

Fig. 2. Detection of brain D-serine by high-performance liquid chromatography with fluorometric detection. The present schemes show representative chromatograms of *N*-tertiary-butyloxycarbonyl-L-cysteine-*o*-phthaldialdehyde derivatives of the authentic standard amino acids (A), the tissues of the cerebral cortex (the neocortical portions) (B) and in the extracellular fluid collected from the medial frontal cortex (C) in the young adult rats obtained by a reversed-phase high-performance liquid chromatographic system with a fluorescence detector [22,24,66]. Routinely, D-homocysteic acid (DHCA) was added as an internal standard in the analysis of the brain tissues (panels B) and of the extracellular fluid (panels C). The panel (C) has been reorganized from the figure published in Ref. [66]. Abbreviations: L-Asn, L-asparagine; D-Asp, D-aspartate; L-Asp, L-aspartate; L-Cys, L-cysfein; L-Gln, L-glutamine; L-Glu, L-glutamate; Gly, glycine; DHCA, D-homocysteic acid; D-Ser, D-serine; L-Ser, L-serine; L-Thr, L-threonine.

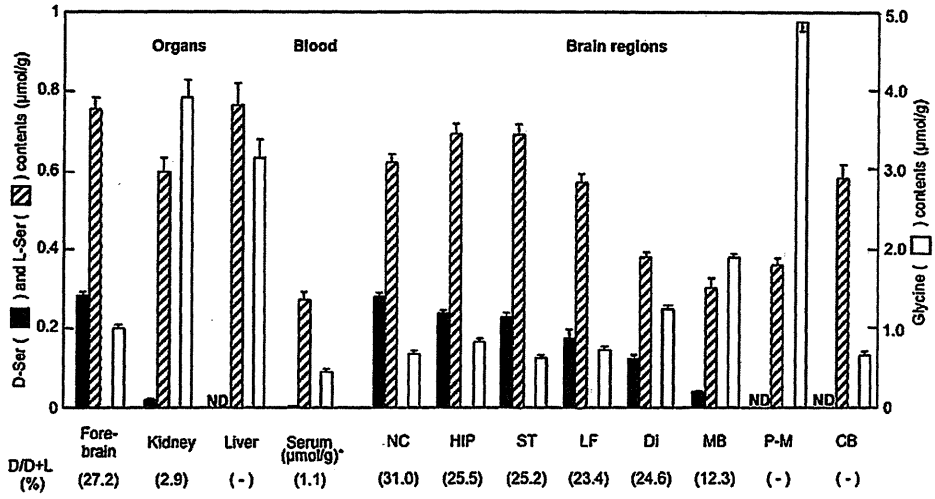

Fig. 3. Contents of D-serine, L-serine and glycine in the various organs, serum and brain regions of the rat. The distribution pattern of D-serine differs markedly from those of L-serine and glycine in the body and brain of the rat [12,22]. The present scheme has been reorganized from the figures published in Refs. [12,22]. Abbreviations: CB, cerebellum; DI, diencephalon (thalamus and hypothalamus); Forebrain (neocortex, paleocortex, striatum, hippocampus and the tissues among them); HIP, hippocampus; MB, midbrain; NC, neocortex; ND, not detectable; P-M, pons–medulla; ST striatum. *Note the unit.

their ratios of D- to total serine are high in regions of the forebrain (contents, 0.35–0.25 μmol/g tissue at the highest level in the cerebral cortex, hippocampus, striatum, etc.; ratios, 31–25%), medium to low in the diencephalon and midbrain (0.19–0.9 μmol/g tissue; 24–12%), and trace in the brainstem and cerebellum [15,22]. The forebrain-preferred distribution pattern of D-serine [15,22,29] has been shown to be strongly correlated with that of the density of the binding sites for glutamate, PCP, and glycine of the NMDA receptor [43,44] and closely resembles the mRNA distribution of the NMDA receptor GRIN2B (NR2B) subunit in particular [45].

The D-serine distribution in the brain changes markedly along with development. Although the distribution in the rodent brain immediately after birth is almost uniform (approximately 0.1 μmol/g), the pattern comes close to that of the maturation period at about three weeks after birth [22,46]. The changes after birth vary with brain regions; the D-serine concentration in the cerebral neocortex reaches the level observed in the maturation period (approximately 0.3 μmol/g) on the postnatal days 21, but, in the cerebellum, it becomes comparable with that of the mature neocortex on the 7th day after birth and then decreases quickly. These changes also correspond with the postnatal development of distribution pattern of GRIN2B mRNA (NR2B) in the brain [22,46,47].

At the cellular level of the mammalian brains, D-serine-like immunoreactivity has been observed in astrocytes in the gray and white matter [29], neuronal cell bodies [36], dendrites [36], axons [36], and microglia [37], and very recently in a small population of oligodendrocytes [48]. These observations are consistent with the quantitative data obtained by HPLC that D-serine contents did not differ between the white and gray matter in the human cerebral neocortex [26]. In addition, Müller cells, astrocytes, and neuronal ganglion cells of the retina has been reported to be positive to the D-serine immunostaining [40].

Phylogenetically, the concentrations of D-serine and the ratios of D- to L-serine contents are extremely low in the brains of fish,

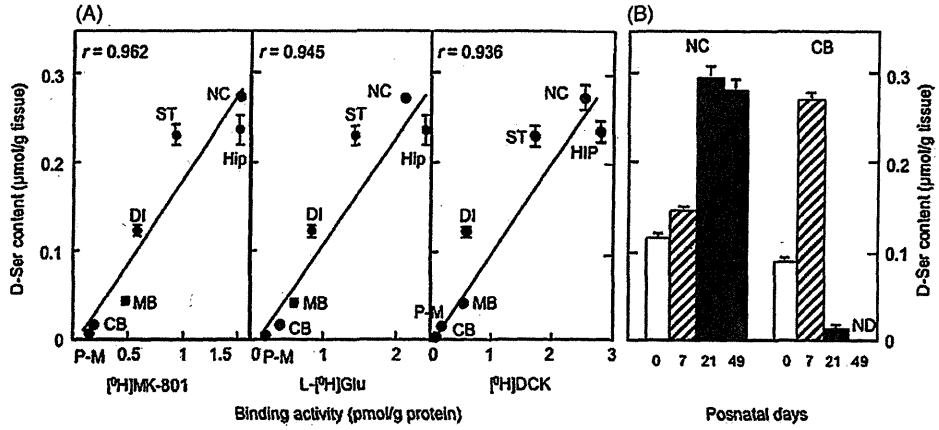

Fig. 4. NMDA receptor-like regional distribution of D-serine in the adult and developing rats. The regional distribution of D-serine contents is closely correlated with that of the densities of the phencyclidine, glycine and glutamate binding sites of the NMDA receptor (panel A) [12,22,43,44] and with the expression levels of its GRIN2B subunit. D-Serine concentrations in the neocortex and cerebellum dramatically change during the postnatal development in a manner observed for the GRIN2B subunit mRNA expression (panel B) [12,22,45,46]. These data indicate that D-serine and various NMDA binding sites and/or the GRIN2B subunit may exhibit similar regional distribution patterns during postnatal development. The limbic forebrain ("LF" in this figure) contains nucleus accumbens, septum, olfactory tubercle and their interstitial tissues. The present schemes have been reorganized from the figures and tables published in Refs. [12,22,43,44,46]. Abbreviations: CB, cerebellum; DI, diencephalon (thalamus and hypothalamus); HIP, hippocampus; LF, limbic forebrain; MB, midbrain; NC, neocortex; ND, not detectable; P–M, pons–medulla; ST striatum.

amphibians, and birds (0.001–0.018 μmol/g tissue; 0.2–1.4%), suggesting that endogenous D-serine is specifically maintained at a high level in the mammalian brain among the vertebrates [49]. It, however, should be noted that the blood of an invertebrate, silkworm, has been reported to exhibit high ratios of D- to total serine contents up to 59% during development [6].

2.3. Synthesis (Fig. 5)

In the rat brain, the existence of serine racemase that synthesizes D- from L-serine was presumed based on the following phenomena: (a) the D-serine concentration is increased when the concentration of L-serine (or glycine) is increased [50]; (b) [^{3}H] L-serine is converted to [^{3}H] D-serine [51]. In fact, pyridoxal 5′-phosphoric acid-dependent serine racemases of rats, mice, and humans, which are activated by ATP or Mg^{2+}, have been isolated [52,53]. The important role of this enzyme in D-serine biosynthesis has been supported by the experiments indicating that (a) immunoreactivity of this enzyme shows a D-serine-like distribution [54] and is detected in both astrocytes and neurons that contain D-serine in the brain [54,55], and (b) the concentrations of D-serine is dramatically decreased by 90% in the brain of its gene knockout mice [56–58] and of the mice with ENU-induced mutation that results in a complete loss of the racemase activity [59]. Moreover, the putative physiological role of L-serine as a precursor for D-serine has indeed been supported by the results that forebrain-specific deletion of the phosphorylation pathway enzyme for L-serine synthesis, D-3-phosphoglycerate dehydrogenase (Phgdh), produced a significant diminution in the cerebral cortical and hippocampal D-serine contents in the mouse [60], suggesting the conversion of L-serine to D-serine mediated by serine racemase. It is also reported that serine racemase is activated by glutamate neurotransmission involving AMPA (α-amino-3-hydroxy-5-methylisoxazole-4-propionic acid) receptors via GRIP (glutamate receptor interacting protein) binding to the enzyme [61].

The physiological functioning condition of the mammalian serine rasemase, however, remains unclear because this enzyme exhibits a serine dehydratase activity higher than racemase activity [55] and shows a serine racemase activity about 1/1000 as low as the alanine racemase of yeast [62] *in vitro*. Moreover, the incomplete depletion of D-serine in the serine racemase gene knockout animals suggests another pathway for D-serine synthesis. From this viewpoint, it is of interest to note that D-serine contents in the postmortem cerebral cortex tissues are markedly decreased in the patients with non-ketotic hyperglycinemia that is caused by the lack of activity of the glycine cleavage system [63] and in the rats treated with an inhibitor of this enzyme system [63]. The possible involvement of the glycine cleavage enzyme system and other serine-related enzymes, such as serine hydroxymethyl transferase and phosphoserine phosphatase, in D-serine biosynthesis is also being studied [63,64].

2.4. Storage

Histochemical studies using a specific anti-D-serine antibody have revealed that D-serine-like immunoreactivity is observed in the astrocytes [29,55], neurons [36,48,55], microglia [37] and oligodendrocytes [48]. The storage sites of D-serine may vary with cell types of the brain.

In the astrocytes of the brain sections, both D-serine antibodies requiring glutaraldehyde-fixation [29,36,48,54] and those optimized for formaldehyde-fixation [37] produce D-serine immunostaining in the vesicular-like structure. In agreement with these observations, the C6 glioma cells and cultured astrocytes obtained from the brain tissue of infant animals seem to have an exocytotic vesicle-like structure to store D-serine, because the immunoreactions of at least D-serine and the synaptic vesicle marker VAMP2 coexist, and because D-serine release is no longer seen with the presence of tetanus toxin that degrades VAMP2 [65].

In contrast, D-serine release in the cultured neurons of the cerebral cortex is not significantly influenced by bafilomycin A1 that inhibits amino acid uptake into the vesicles [55], although D-serine-like immunoreactivity is reported in the vesicular-like structures in the neurons located in the hindbrain regions [37]. Together with the observations that D-serine is not transported into purified synaptic vesicles under conditions optimal for the uptake of known transmitters, these results suggest that the neuronal D-serine may be mainly stored in the cytoplasm [55].

Further investigation is needed to clarify the exact storage structures for endogenous D-serine and their molecular machineries in the astrocytes, neurons, and also in the other cells that exhibit the immunoreactivity to D-serine.

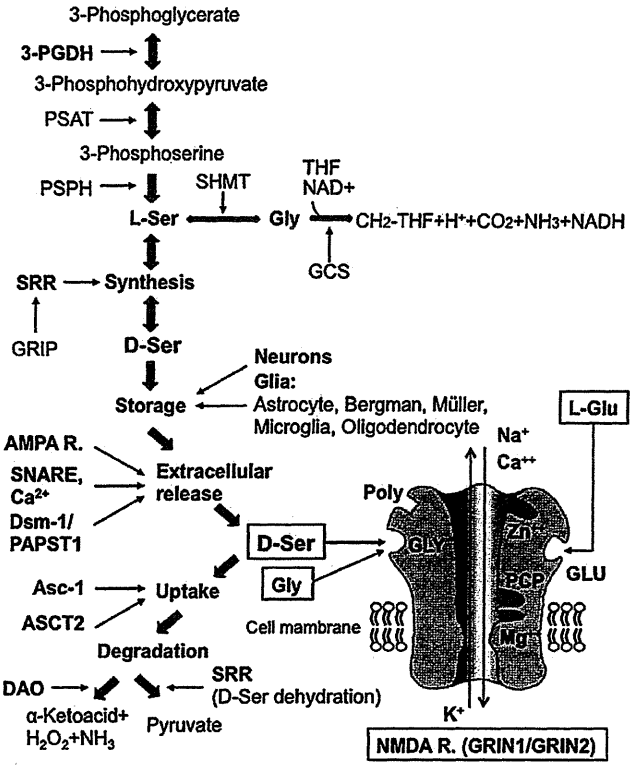

Fig. 5. Schematic representation of the presumed metabolic pathways for D-serine in the mammalian nervous systems. The candidate molecules or cells for the respective metabolic or functional processes of intrinsic D-serine in the mammalian nervous systems including the retina are summarized. However, most of their precise roles and cellular localization still await further elucidation. It is well established that D-serine acts on the glycine site of the *N*-methyl-D-aspartate type glutamate receptor (NMDA R.) consisting of GRIN1 (NR1) and GRIN2 (NR2) subunits. The NMDA receptor complex has the multiple regulatory binding sites for glutamate (Glu), glycine and D-serine (Gly), magnesium ions (Mg^{++}), phencyclidine (PCP), and polyamine (Poly). The oligomeric NMDA receptors form tetrameric channels comprising two copies each of GRIN1and GRIN2 subunit. D-Serine has also been indicated to interact with the NMDA receptor containing GRIN1 and GRIN3 subunits and δ2 glutamate receptor that are not shown in this scheme. Abbreviations: AMPA R., α-amino-3-hydroxy-5-methyl-4-isoxazolepropionic acid receptor; Asc-1, Na^+-independent alanine–serine–cysteine transporter 1; ASCT2, Na^+-dependent broad-spectrum neutral amino acid transporter 2; DAO, D-amino acid oxidase; D-Ser, D-serine; Dsm-1/PAPST-1, D-serine modulator-1/3′-phosphoadenocine 5′-phosphosulfate transporter-1; GCS, glycine cleavage system; Gly, glycine; GRIP, glutamate receptor interacting protein; L-Glu, L-glutamate; NMDA R., *N*-methyl-D-aspartate type glutamate receptor; 3-PGDH, 3-phosphoglycerate dehydrogenase; PSAT, phosphoserine aminotransferase; PSPH, phosphoserine phosphatase; SHMT, serine hydroxymethyltransferase: SNARE, soluble *N*-methylmaleimide susceptibility factor attachment protein receptor; SRR, serine racemase; THF, tetrahydrofolate.

2.5. Extracellular release (Fig. 5)

As predicted by characteristics of endogenous D-serine that are high affinity and selective ligand properties for the NMDA receptor glycine site and a NMDA receptor-like tissue distribution in the brain, D-serine has been demonstrated to be present in the extracellular fluid of the brain regions of a freely moving animal by using an *in vivo* microdialysis technique [22,66]. The extracellular concentrations, like tissue contents, show a strong correlation with the densities of the NMDA receptor (approximately 5×10^{-6} M in the frontal cortex one of the portions that contain the highest levels) [66]. For the investigations of the control mechanisms underlying the extracellular D-serine dynamics, *in vitro* methods including brain slice and homogenate, primary culture and cell line preparations, retina and the Xenopus oocytes expression system have been successfully applied as well.

The concentrations of brain extracellular D-serine appears to be under a distinct regulation from those of classical neurotransmitters based upon the data obtained from *in vivo* dialysis experiments. Thus, unlike glutamate, glycine and dopamine, the amount of D-serine in the frontal extracellular fluid was not increased, but rather decreased, by depolarization caused by veratrine or high concentrations of potassium ion [66]. Although a recent *in vivo* extracellular amino acid monitoring revealed a small and transient enhancement of D-serine levels in the striatum after a veratridine and high potassium application, this change is dissimilar to those observed in classical neurotransmitters in the magnitude and the feature followed by an immediate and lasting reduction [67]. Furthermore, the interruption of the nerve impulse flow or removal of extracellular calcium ions failed to reduce the extracellular D-serine levels [66]. The differential effects of the altered neuronal activity support the idea that not only neurons but also certain glial cells could participate in the regulation of the extracellular D-serine [66]. A reversible glia-selective toxin, fluorocitrate, indeed attenuated significantly the extracellular contents of D-serine with complete loss of extracellular glutamine that is derived from the glial cells but not neurons [68]. Furthermore, retinal release of D-serine has been found to be contingent upon glial cell activity [69].

In vitro studies using astrocytes [29,61,65] or neurons [55] in primary culture, C6 glioma cells [65,67] and retina [69] indicate that the extracellular release of D-serine is increased by glutamate, AMPA (alpha-amino-3-hydroxy-5-methyl-4-isoxazolepropionic acid), or kainic acid whereas NMDA and kainic acid have been observed to down-regulate the D-serine release in an *in vivo* system [70]. Glutamate-induced D-serine release in cultured astrocytes and C6 cells depends on intra- and extracellular Ca^{2+} and SNARE (soluble N-methylmaleimide susceptibility factor attachment protein receptor) and is suppressed by an inhibitor of the uptake of amino acids into the synaptic vesicles; therefore, it is presumed to be mediated by the exocytotic processes of synaptic vesicle-like structures [65]. In the astrocyte in primary culture, AMPA-induced release of D-serine is attenuated by volume-regulated anion channel blockers [67]. It is also reported that addition of micromolar concentrations of L-alanine or L-serine induces robust release of D-serine from astrocytes, but not from neurons [71]. In this releasing effect, L-serine is more effective than kainite [71]. Together with the fact that the efflux of D-serine via ASCT2 by ASCT2 substrates can also be demonstrated using the *Xenopus laevis* oocyte expression system [72], these phenomena suggests that D-serine release from astrocytes may be mediated by amino acid heteroexchange catalyzed by the neutral amino acid transporter ASCT rather than stimulation of the non-NMDA receptor [71]. Retinal D-serine efflux could similarly be originated from the Müller glial cells through the ASCT2 because (a) AMPA-evoked D-serine release from the retina persisted in the presence of neural inhibitors, tetrodotoxin and cadmium chloride, but was abolished after application of a glial toxin, α-aminoadipic acid, [69] and (b) a retinal Müller cell line and primary cultures of mouse Müller cells express serine racemase and ASCT2 [72].

In primary neurons, D-serine release evoked by glutamate receptor agonists depends on extracellular Ca^{2+}, but it is not decreased by the removal of intracellular Ca^{2+} or a potent inhibitor of vesicular neurotransmitter uptake [55], and depolarization (veratridine)-evoked release of D-serine does not require internal or external Ca^{2+}, suggesting an unknown nonvesicular release mechanism in a cytosolic route [55]. Finally, a depolarizing stimulus, veratridine or high potassium, increases the release of D-serine in primary neurons, but not in primary astrocytes [55].

The above findings indicate that the molecular mechanisms of D-serine release differ between glial cells and neurons, and could be diverse in the respective cell types. The inconsistent results

between *in vivo* and *in vitro* studies may, at least in part, be due to their distinct conditions in the cellular interactions and neuronal circuits. Therefore, the exact molecular and cellular setups of the release machinery for D-serine await further elucidation. In this point, it is proposed that rat dsm-1 gene [73], an ortholog of human 3′-phosphoadenosine-5′-phosphosulphate transporter-1 gene and its protein product could be candidates for the members of the molecular cascade regulating intra- and extra-cellular contents of brain D-serine, because (a) dsm-1-expressing oocytes diminishes the sodium-dependent and -independent accumulation of D-serine and the basal levels of the intrinsic D-serine and increases the rate of release of the pre-loaded D-serine [73] and (b) dsm-1 mRNA has a D-serine-like distribution in the rat brain [73]. It is also noteworthy that, in the hippocampus, ephrinBs that are transmembrane proteins and known to regulate synaptic transmission and plasticity have been shown to regulate D-serine synthesis and release in astrocytes through activating EphB3 and EphA4 receptors that interact with PICK1 (protein interacting with C-kinase) and protein kinase Cα [74].

2.6. Receptor (Fig. 5)

D-Serine was initially described as a selective ligand for the strychnine-insensitive glycine binding site of the *N*-methyl-D-aspartate (NMDA) type glutamate receptor in the 1980s [19]. Because (a) D-serine mimic the agonistic effects of glycine on the NMDA receptor, (b) it displays a low affinity (high μM order) for the strychnine-sensitive inhibitory glycine receptor and a negligible binding capacity for the other glutamate receptors, and (c) its high binding affinity for and stimulating effects on the glycine site of the NMDA receptor are highly stereoselective, the D-amino acid has been used as an excellent tool for the functional study of the NMDA receptor in the mammalian central nervous system [19]. Cristal structural analysis has revealed that D-serine binds to the GRIN1 (NR1) subunit S1S2 ligand-binding core like other glycine site full and partial agonists and antagonists such as glycine, D-cycloserine and 5,7-dichlorokynurenic acid [75,76]. Further, using ligand binding assay, crystallographic analysis and all-atom molecular dynamics simulations, the GRIN3 (NR3) subunit that is a more recently identified class of the NMDA receptor subunits family composing a functional receptor with the GRIN1 subunit has been revealed to have the ligand biding domain for D-serine and glycine with higher affinity than GRIN1 [77]

The δ2 type glutamate receptor, which is predominantly expressed in the cerebellum, has recently been found to bind D-serine with K_d values of approximately 1 mM [78]. There are so far no other established receptor sites that have a relatively high affinity for D-serine. However, a NMDA glycine site antagonist-insensitive binding site that is detected in the brain synaptosomes and show the affinity for D-serine at high nanomolar range and brain-preferring distribution could compose a novel target molecule for D-serine [79].

2.7. Uptake (Fig. 5)

The substantial uptake of radioactive D-serine is observed in the homogenates of the rodent cerebral cortex and cerebellum [80,81], primary astrocytes and neurons obtained from the cerebral cortex of rodents [29,82], and C6 cells of rat glioma origin [83,84]. By contrast, there is a very low level of tritiated D-serine uptake activity in the homogenates of the peripheral tissues such as liver and kidney [80]. D-Serine was not transported into purified synaptic vesicles under conditions optimal for the uptake of known transmitters [55], and the pharmacological properties of uptake are different from those of previously reported transporters [55] [88], indicating the existence of a novel carrier that transports D-serine into cells in the central nervous system. Already-described molecules expressed in the brain, having the ability to take up D-serine at the μM order, include sodium-dependent neutral amino acid transporters ASCT1 and ASCT2 [72], the sodium-independent neutral amino acid transporter Asc-1 [85,86], and the proton-dependent amino acid transporter PAT1 [87]. Among these, Asc-1 [85,86] has the highest affinity for D-serine (IC_{50} of approximately 10–50 μM), is distributed widely in the brain, and occurs mainly in presynaptic nerve terminals. In addition, D-serine incorporation in the cerebral cortex and cerebellum of Asc-1 knockout mice is decreased to about 1/3 or below, suggesting the possible involvement of Asc-1 in physiological D-serine transport [86]. ASCT2 is immunohistochemically demonstrated in the dendrites of neurons of the cortex, hippocampus and striatum, but not in their cell bodies and astrocytes, in the brain sections [81]. This observation is supported by the data that low affinity ($K_T > 1$ mM) sodium-dependent D-serine and L-glutamine uptake characteristic of ASCT2-mediated transport was observed in the cortical P2 synaptosomal preparations [81]. In cortical neuron and astrocyte primary cultures, ASCT2-like uptake activity and immunoreactivity has also been found, noting the differential contribution of ASCT2 to the low affinity uptake of D-serine in physiological [81] and cultured astrocytes [82].

D-Serine uptake in an intact retina tissue, a Müller cell line or primary cultures of mouse Müller cells has been shown to be sodium-dependent and blocked by L-alanine, L-threonine, L-cysteine, L-serine, glutamine, or asparagine, but not anionic amino acids or cationic amino acids, suggesting that D-serine transport in Müller cells occurs via ASCT2 rather than ASCT1 or $ATB^{0,+}$ [72]. Indeed, RT-PCR assay confirmed the expression of ASCT2, but not $ATB^{0,+}$, mRNA in Müller cells, and immunoblotting and immunohistochemistry also detected ASCT2 in retinal sections and in primary cultures of mouse Müller cells [72].

2.8. Degradation (Fig. 5)

D-Amino acid oxidase (DAO) is an only mammalian enzyme that is proven *in vivo* to degrade D-amino acids containing D-serine [88]. In fact, a mutant mouse strain lacking DAO activity contains much higher contents in the brain of D-serine and D-alanine, which are selective substrates for DAO, than the corresponding normal mouse strain [27,89]. D-Serine deaminase [9], D-serine dehydratase [8] and serine rasemase [90] are also able to break down D-serine. However, absence of the two former enzymes in the mammalian tissues and no increase in the D-serine contents in the serine rasemase deficient mice [56,57,59] are argued against their physiolocal roles as D-serine degrading enzymes.

The distribution pattern of DAO gene and protein expression in the brain is inversely correlated with that of D-serine contents [91]. Brain DAO activity in the rodents is detectable and increased rapidly in the cerebellum, pons, and medulla oblongata around the postnatal days 10 [88] when the D-serine concentration starts to decrease in these brain areas [46]. Expression of the DAO gene is noted in cultured astrocytes from the rat cerebral cortex [92] although the activity and gene or protein expression of DAO in the forebrain are very low or undetectable. The D-serine content of mutant mice lacking this enzyme activity is minimally and dramatically increased in the cerebral cortex and the cerebellum, respectively [27,89]. Therefore, DAO is presumed to degrade D-serine at least in the hindbrain and it cannot be denied that the molecules other than DAO might be involved in the physiological elimination of the D-serine in the forebrain. It is also possible that DAO could play a significant role in forming a characteristic concentration gradient of D-serine in the brain [30].

2.9. D-Serine-responsive molecules

The genes or their protein products whose expressions are selectively induced by D-serine, but not by L-serine seem to be candidates for the molecules related to the receptor-intracellular signal transduction systems or metabolic pathways for D-serine. For instance, previously unreported transcripts that have a stereoselective response to D-serine, dsr-1 (D-serine-responsive transcript-1) [93] and dsr-2 [94] were isolated from the rat cerebral neocortex. A part of dsr-1 is homologous to the M9.2 gene encoding the proton ATPase subunit, which may be involved in the incorporation and release of D-serine [93]. dsr-2 [94] shows a similar distribution in the brain to those of D-serine and NR2B during postnatal development, and the gene has been mapped to the opposite strand of the neurexin-3α gene that has been indicated to be associated with NMDA receptor regulation, suggesting a functional correlation with D-serine or the GRIN2B (NR2B) subunit.

3. Physiological functions of D-serine

Pharmacological, molecular and cellular biological, electrophysiological, and histochemical analyses have suggested that, in the mammalian central nervous system, endogenous free D-serine plays a major role in the regulation of the NMDA type glutamate receptor and of glia–neuron interaction and may, at least in part, participate in the control over the δ2 type glutamate receptor and the neural development.

3.1. Regulation of the glutamate receptors

3.1.1. NMDA receptor

3.1.1.1. GRIN1/GRIN2 (NR1/NR2)-type NMDA receptors (Fig. 5). D-Serine selectively stimulates the glycine-binding site of the NMDA receptor, consisting of GRIN1 and GRIN2A-D subunits, to facilitate the following actions of glutamate via this receptor [19]: (a) depolarization, (b) inward electric current, (c) Ca^{2+} influx, (d) cGMP production, (e) release of various neurotransmitters, and (f) neuronal cell death. These actions are shared with glycine and D-alanine, characterized by stereospecificity that is barely seen in L-serine and L-alanine. The facilitating influence is considered to result from the increased frequency of channel opening, based on the phenomena that D-serine and other glycine site agonists augment the radiolabelled ligand binding to the phencyclidine regulatory site within the ionic channel [19].

Stimulating the glycine-binding site alone cannot produce an excitatory postsynaptic membrane potential; however, it is obligatory required for the generation of sufficient neurotransmission by glutamate. Therefore, the glycine site agonists such as glycine, D-serine, and D-alanine are referred to as coagonists of the NMDA receptor [19,30]. Together with the strong neuroanatomical correlates between D-serine and NMDA receptor, especially GRIN2B subunit, in the brain, the aforementioned characteristic actions of D-serine on the NMDA receptor suggest that D-serine in the brain is a physiological coagonist of the GRIN1/GRIN2 (NR1/NR2) type receptor [12,15,22,30]. In consonant with this idea, the selective elimination of endogenous D-serine by means of application of D-amino acid oxidase or D-serine deaminase without affecting the glycine contents in the brain slice, the primary neurons or the mixed primary culture system of glial cells and neurons causes a marked attenuation in the following functions of the GRIN1/GRIN2 type NMDA receptor *in vitro*: the nitric oxide synthetic-enzyme activation [95], the induction of NMDA receptor-dependent long-term potentiation (LTP) [96], and the NMDA-elicited excitotoxicity [55]. It is also well accepted that the NMDA type glutamate receptors play pivotal roles in the control of the neural plasticity, learning and memory, behavioral responses, neuronal cell death *in vivo* at the individual levels. The facts that the various serine racemase deficiency mice displaying a marked loss of D-serine contents in the brain show the disturbances or changes in the above NMDA receptor-mediated functions such as spatial memory [57,59], memory for order [58] and NMDA neurotoxicity [56] add a further support the physiological coagonist actions of D-serine on the NMDA receptor.

The extracellular contents of D-serine and another intrinsic NMDA receptor coagonist glycine exceed those fully activating the glycine site of the NMDA receptor. However, the glycine site may not always be saturated under physiological conditions [97] because the NMDA receptor currents in the rat prefrontal area are enhanced when a selective inhibitor of the glial glycine transporter GLYT1 (N [3-(4′-fluorophenyl)-3-(4′-phenylphenoxy)propyl]sarcosine (NFPS)), which elevate the synaptic glycine levels, or D-serine (50–100 mg/kg iv) is administered systemically [97].

Then, the important question arises as to the possible differences in the physiological roles of D-serine and glycine as the coagonists for the NMDA receptor (Table 1). It can be presumed from the divergent distribution patterns of D-serine, glycine and four types of NR2 subunits that D-serine and glycine could have the distinct modes of actions to the four sorts of heteromeric NMDA receptors comprising GRIN1 and any one of GRIN2A to GRIN2D subunit. In each type of the heteromeric receptors expressed on the Xenopus oocyte, D-serine exhibits a several-fold stronger reinforcing effect on the glutamate-induced inward current than glycine [98]. Although there is no obvious discriminations in the influences of each amino acid on the four kinds of the heteromeric receptors [98], the differential regulations of extracellular signals between these two amino acids are pointed out by the *in vivo* dialysis experiments showing that a glia toxin, fluorocitrate [68], diminishes the frontal extracellular contents of D-serine with an increase in those of glycine, and D-cycloserine [99] produced an elevation and no alteration in the frontal D-serine and glycine contents in the dialysates, respectively. To clarify the exact cellular and molecular mechanisms underlying the release of D-serine and glycine would provide a critical clue for the biological significance of the dual coagonists for the NMDA receptor.

3.1.1.2. GRIN1/GRIN3-type NMDA receptors. GRIN3 subunits of the glutamate receptors are the lease characterized members of the NMDA receptor gene family and found to show the distinct ligand responses from GRIN2 subunits [100]. Neuroanatomical analyses have revealed in the rat that expression of the GRIN3A subunit is widely observed through the brain and spinal cord with peaking around early postnatal stage while GRIN3B is expressed predominantly in motor neurons in the brainstem and spinal cord.

Unlike GRIN1/GRIN2-type NMDA receptors, the GRIN1/GRIN3A or GRIN1/GRIN3B heteromeric NMDA receptors are excited by glycine, but not glutamate or NMDA (inward electric current) [100] in the Xenopus oocytes expression system or cerebral cortical neurons. An antagonist to the glutamate-binding site or PCP-binding site does not affect this glycine-induced electric current; however, it is suppressed by a selective agonist and antagonist for the glycine-binding site, D-serine and 5,7-dichlorokynurenic acid, respectively [100]. In contrast to glycine, D-serine alone has been reported to fail to or partially activate the GRIN1/GRIN3A or GRIN1/GRIN3B-type NMDA receptors expressed in the Xenopus oocytes or the HEK 293 cells [100]. Further, D-serine as well as glycine, in the absence of glutamate agonists induce excitatory responses in a NMDA glycine site antagonist-reversible and a glutamate-site antagonist-insensitive fashion in optic nerve myelin, and no longer produce this response in GRIN3A-deficient mice [101]. These data are consistent with